Master thesis

Removal of active pharmaceutical ingredients from wastewater by application of nanobubble technology and ultraviolet light

June 9_{th} 2023

AALBORG UNIVERSITY
STUDENT REPORT

AALBORG UNIVERSITY
STUDENT REPORT

Department of the Built Environment,
Water and Environmental Engineering
Thomas Manns Vej 23
9220 Aalborg East
https://www.byggeri.aau.dk/

Title:

Removal of active pharmaceutical ingredients from wastewater by application of nanobubble technology and ultraviolet light

Project:

Master thesis

Project period:

Septemper 1_{st} 2022 - June 9_{th} 2023

Participants:
Vibeke Kirstine Hansen
Klara Wanstrup

Supervisors:

Morten Lykkegaard Christensen
Mads Koustrup Jørgensen
Asbjørn Haaning Nielsen

Number of pages: 87
Ended: 9/06/2023

.

Preface

This is a masterthesis written by two students of Water and Environmental Engineering from the Department of Built Environment at Aalborg University. The project was commenced in September 2022 and and concluded in June 2023. The project comprises elements from the field of chemistry as well as environmental engineering. All experiments were conducted at the Department of Chemistry and Bioscience.

We would like to thank our supervisors Asbjørn Haaning Nielsen from the Department of Built Environment, Morten Lykkegaard Christensen and Mads Koustrup Jørgensen from the Department of Chemistry and Bioscience for their optimism and constructive feedback during the course of the project. We also give credit to Mette Haferbier from the Department of Chemistry and Bioscience for her assistance with experiments and her positive spirit.

Also thanks to Moleaer and Techras Nano for feedback and for making the nanobubble generator available for this project. Some adjustments made in relation to the experiments were based on input from the supplier of the equipment. This will be clearly referenced in the report.

Finally we would like to recognise Morten Boel Overgaard Andersen for his crucial support in the start-up phase of this project.

It has been an interesting and challenging study of a novel topic in the field of wastewater and a steep learning curve in the discipline of chemistry.

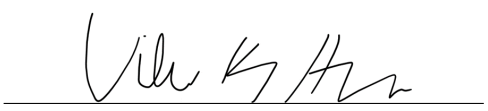

9/6-23 Vibeke Kirstine Hansen

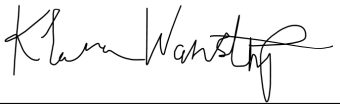

9/6-23 Klara Wanstrup

Abstract

The problem of active pharmaceutical ingredients (APIs) found in the effluent of wastewater treatment plants and thereby in the water environment is of rising concern. Therefore this project have looked at an alternative and more environmental friendly method for removal of pharmaceuticals compared to already known methods e.g. ozonation and activated carbon technologies. Nanobubbles and their ability to make oxidative reactions caused by exposure to UV light was investigated. The thesis is that by destabilising nanobubbles in an aqueous solution, the formation of hydroxyl radicals will oxidate the APIs.

Size distributions and zeta potential measurements based on dynamic light scattering (DLS) was used as a method of documenting nanobubbles in clean water samples. A combination of O_2 and demineralised water where salts has been added to increase ion strength in the solution yielded the most consistent results. Size distributions ranged from 256 $\pm$116 nm to 484$\pm$32 nm and zeta potential measurements between -13 mV and -20 mV indicated that the DLS method can be used to document nanobubbles in clean water samples.

A modified Winkler titration method was tested to document nanobubbles in environmental water samples. By decreasing the pH in the solution nanobubbles collapse and as a result dissolved oxygen (DO) should increase. After two days DO increased from 8.45 mg L^{-1} to 10 mg L^{-1} and after seven days it increased to 11.6 mg L^{-1}.

The oxidative capacity of nanobubbles has been tested by looking at the degradation of methylene blue as an indicator substance. No consistent degradation of methylene blue was detected.

Degradation of two APIs often found in the effluent of Danish wastewater treatment plants was tested; Diclofenac and venlafaxine. Diclofenac was primarily degraded by the UV light with an average removal over an hour of approximately 84.7% for UV light and nanobubbles and 81.8% for UV light alone. Venlafaxine was less sensitive to UV light in terms of degradation. When exposed to nanobubbles and UV light the average removal of venlafaxine over an hour was 6.35% and when exposed to UV light alone the average removal over an hour is 4.82%.

Table of contents

List of acronyms

API	Active pharmaceutical ingredients
AUH	Aarhus University Hospital
BOD	Biochemical oxygen demand
DANVA	The Danish Water and Wastewater Association
DLS	Dynamic Light Scattering
GAC	Granular activated carbon
HPLC	High-performance liquid chromatography
NOVANA	National Aquatic Environment and Nature Monitoring Programme
NTA	Nanoparticle Tracking Analysis
OUH	Odense University Hospital
PAC	Powdered activated carbon
PEC	Predicted environmental concentration
PNEC	Predicted no effect concentration
QTOF	Quadrupole time-of-flight (mass spectrometry)

1 Introduction

In recent years focus on micropollutants such as pharmaceuticals in the water environment has increased. The concern is the potential harmful impact the substances may have on public health as well as the ecological status of streams, lakes and coastal waters.

The increased awareness can be exemplified by the European watch list for surface water under the Water Framework Directive [Loos et al., 2018]. Chemicals of emerging concern are selected for the watch list for four years or until sufficient data is gathered. The purpose of this is a knowledge based risk assessment of whether or not regulation is well-founded. This collection of data is anchored in national surface water surveillance such as National Aquatic Environment and Nature Monitoring Programme (NOVANA) in Denmark [DCE and GEUS, 2017]. In October 2022 a proposal for the revision of the European urban wastewater treatment directive was published. This included a minimum requirement of 80% for the removal of selected pharmaceuticals [Directorate General for Environment, n/a].

In a Danish context, a decision was made in 2007 to construct six large regional hospitals to centralise specialised patient care. This has led to a review of the hospital wastewater permits. In Aarhus an investigation was conducted into the discharge of active pharmaceutical ingredients (API) in the wastewater effluent from Aarhus University hospital (AUH) relative to the total catchment area to Egaa wastewater treatment plant. AUH accounts for 13% of the pharmaceuticals, whereas the remainder mainly stems from private households [Bailon et al., 2021]. This trend has presumably increased over the years with the increase in ambulatory treatment and subsequent decline in inpatient treatment [Bailon et al., 2021]. Hence this supports the notion of a centralised wastewater treatment solution to account for the API from private households.

Finally, developments in the field of water sample analysis has lead to the recent discovery of harmful substances in drinking water wells and wastewater treatment plant effluents. In addition to target analysis of specific substances, simultaneous screening of multiple substances is now possible using non-target analysis based on e.g. the QTOF technology [Eurofins, n/a]. This technology has e.g. been used at Skanderborg utility company for mass screening of pharmaceuticals in the influent and effluent flow to determine the removal efficiency of the treatment process [Bayley, 2022].

Current practice in the EU for the removal of pharmaceuticals is the use of ozone or activated carbon as a final polishing stage [The Danish Environmental Protection Agency, 2022]. Ozonation has demonstrated removal efficiency $> 85\%$ of API [Jensen et al., 2022], but it has a number of disadvantages e.g. a high energy consumption and the potential

formation of bromate above a threshold of 0.15 mg/L bromide in the water [Stapf et al., n/a]. This is particularly problematic in Denmark, due to the proximity to the coastline as seewater intrusion may lead to increased bromide concentrations in groundwater and sewer systems [Stapf et al., n/a; DANVA, n/a]. The activated carbon technologies GAC (granulated activated carbon) and PAC (powder activated carbon) has a high removal rate for most APIs [The Danish Environmental Protection Agency, 2022]. A removal effeciency $> 75\%$ has been demonstrated [The Danish Environmental Protection Agency, 2021], while the adsorption efficiency of other API e.g. sulfamethoxazol can be as low as 7% depending on the bed volume [The Danish Environmental Protection Agency, 2021]. In addition to the varying efficiency of adsorption, the disadvantages of activated carbon filters include an energy consuming production. Furthermore GAC has to be regenerated outside of Denmark, whereas PAC cannot be regenerated and has to be disposed of [The Danish Environmental Protection Agency, 2022]. Finally, the activated carbon often come from unsustainable sources and must be transported long distances to the point of application [The Danish Environmental Protection Agency, n/a]. Hence the sustainability perspective of activated carbon filters is gloomy with the current practice. Both ozonation and PAC need additional consideration in terms of work environment [The Danish Environmental Protection Agency, 2021].

An emerging technology in the field of wastewater treatment is the nanobubble technology. Bulk nanobubbles are cavities of gas in a an aqueous solution with a diameter less than 1 μm [Michailidi et al., 2020], but this term is often applied interchangedly with the definition of smaller bubbles having a diameter less than 200 nm [Moleaer, n/aa; Meegoda et al., 2018; Yasui et al., 2018]. Nanobubbles can be generated using a number of methods including cavitation, electric or shearing from a porous surface such as a membrane [Moleaer, n/ac]. Nanobubbles are believed to have a number of applications as presented in Figure 1.1.

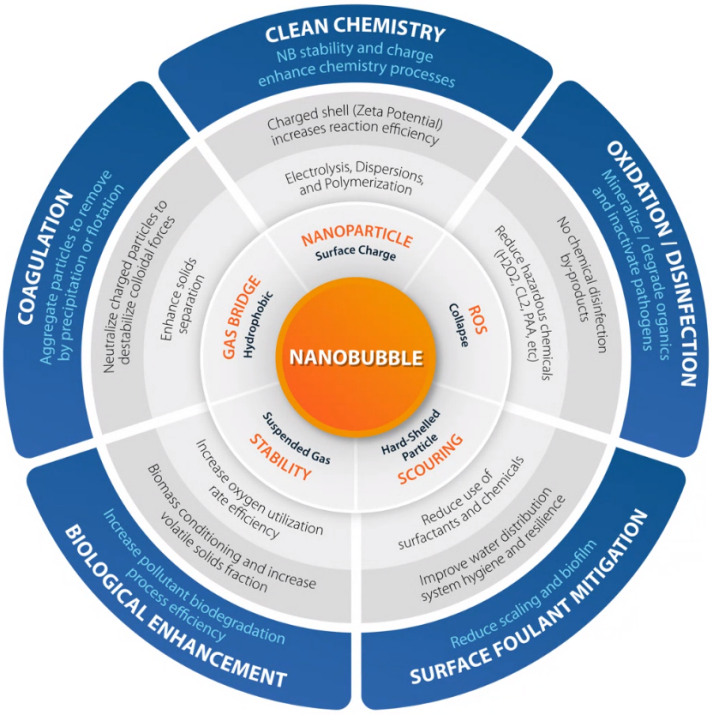

Figure 1.1.Potential applications of nanobubbles [Moleaer, n/ac]

Few of these applications are well understood or documented. It is believed that reactive oxygen species (ROS) can be generated when nanobubbles collapse as a result of an exogenous force e.g. sonication or UV light [Takahashi et al., 2017; Liu et al., 2016]. ROS such as hydroxyl radicals are non-selective and highly reactive [Dutta et al., 2001], hence a potential for the degradation of micropollutants. This report will investigate the oxidative capacity of nanobubbles from shear in comination with UV and the potential for degradation of API.

1.1 Research questions

Can nanobubbles exposed to ultraviolet light form reactive oxygen species and degrade active pharmaceutical ingredients?

- How can nanobubbles in water and wastewater samples be documented?
- How can the formation of hydroxyl radicals be documented?

1.2 Methodology

APIs included in this project are selected based on a literature study of measurement campaigns at Danish wastewater treatment plants. The focus will be on concentrations of APIs that often exceed the predicted no-effect concentration (PNEC) value in wastewater effluents. The environmental risk of the APIs i.e. the PNEC in relation to the predicted environmental concentration (PEC) is not included in this study as this will require specific knowledge about local conditions such as dilution.

Nanobubbles are formed by shearusing a Moleaer Lotus unit. The nanobubbles are detected using a Malvern Nano ZS zetasizer documenting size distributions and zetapotential of the water samples. Futhermore an attempt to will be made to develop an alternative method to document the nanobubbles using a modified Winkler method.

The formation of ROS caused by the sudden collapse of nanobubbles is examined by exposure to UV light at 254 nm. Different experimental setups will be attempted varying flow and volume. Based on these tests a experimental setup for the degradation of APIs will be selected. Two indicators of hydroxyl radicals will be tested; benzoic acid and methylene blue dye. Hydroxyl radicals will be formed using the Fenton reaction to test the application of the two indicators.

Tests of API degradation will be measured using a Dionex HPLC with UV detection and a Phenomex Kinetex EVO C18 column.

2 Nanobubbles

2.1 Properties of nanobubbles

Nanobubbles are gas filled cavities containing atmospheric air, oxygen or any other type of gas. The size definition can vary according to different sources, e.g. according to Meegoda et al. [2018] and Moleaer [n/aa] the definition of nanobubbles is a diameter below 200 nm, but a typical definition of nanobubbles is a diameter below 1 μm [Michailidi et al., 2020] [yu Zhang et al., 2020]. An additional subcategory of nanobubbles are ultrafine bubbles defined as having a diameter of approximately 100 nm [AlHesibri et al., 2016]. Figure 2.1 shows the size classification of smaller bubbles.

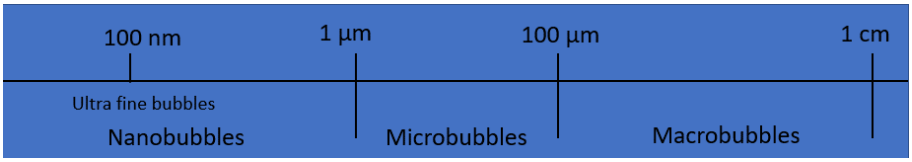

Figure 2.1.Size classification from ultra fine bubbles to macrobubbles.

Nanobubbles have many fields of applications such as wastewater treatment and agriculture due to their stability and the potential reactivity when bubbles collapse, compared to macro- and microbubbles [Atkinson et al., 2019]. Nanobubbles have a higher stagnation time in solutes compared to macrobubbles which is an advantage in terms of e.g. mass transport efficiency, absorption and chemical reactions at the gas-liquid interface [Meegoda et al., 2018]. The fate of bubbles is related to the size i.e. the larger the bubble the faster the bubble will shrink and eventually disappear [Agarwal et al., 2011]. Brownian motions governs the movement of nanobubbles whereas for larger particles buoyancy is the dominating force. Nanobubbles with a size below 1 μm is driven by Brownian motions whereas particles with a size above 1 μm is driven by buoyancy, hence nanobubbles have a neutral buoyancy [Moleaer, n/ac].

Nanobubbles can exist in bulk solutions as well as attached to surfaces. This project has a focus on bulk nanobubbles. Although there seems to be consensus on the higher stability of nanobubbles relative to micro- and macrobubbles, it is still debated whether nanobubbles can stay suspended for days [Kikuchi et al., 2009], weeks [Meegoda et al., 2018] [Azevedo et al., 2016] or even months [Yasuda et al., 2019].

2.2 Gas and pressure theory

2.2.1 The Ideal Gas Law

The Ideal Gas Law is an approximation of the behavior of gasses resulting from changes in pressure and temperature. The Ideal Gas Equation can be used to calculate the oxygen added to the water as well as the nanobubbles. More on this in Section 2.5.1. The Ideal Gas Equation is shown in Equation 2.1 [Harris and Lucy, 2019].

$$p \cdot V = n \cdot R \cdot T \tag{2.1}$$

where:

p	Pressure in $[Pa]$
V	Volume in $[m^3]$
n	Numbers of moles [-]
R	Gas constant in $[\frac{J}{mol \cdot K}]$
T	Temperature in [°K]

2.2.2 Young-LaPlace equations

The Young-Laplace is an equation that relates to the pressure difference across the interface of two fluids, e.g. water and air, to the curvature of the interface [Behroozi, 2022] [AlHesibri et al., 2016]. The Young-Laplace equation is shown in Equation 2.2

$$\Delta P = \frac{2 \cdot \gamma}{r} \tag{2.2}$$

where:

ΔP	Internal pressure $[Pa]$
γ	Surface tension $[N\, m^{-1}]$
r	Bubble radius $[m]$

The properties of the gas bubble depends on the surface charge on the bubble surface. It is under neutral pH-conditions that this applies as the nanobubble surface is negatively charged which is due to the concentration OH^- ions on the gas-water interface of the bubble [Meegoda et al., 2018]. To account for this a modified Young-Laplace equation has been suggested by Meegoda et al. [2018] and Liu and Guoxin [2016]. The equation is shown in Equation 2.3. According to Meegoda et al. [2018] the pressure difference is a results of the surface tension ($\frac{2 \cdot \gamma}{r}$) being reduced by the surface charge ($\frac{\sigma^2}{2 \cdot D \cdot \varepsilon_0}$). Even though the surface charge reduces the surface tension, the internal pressure is getting larger, as the surface charge of nanobubbles is negative at neutral pH in clean water [Agarwal et al., 2011][Atkinson et al., 2019].

$$\Delta P = \frac{2 \cdot \gamma}{r} - \frac{\sigma^2}{2 \cdot D \cdot \varepsilon_0} \tag{2.3}$$

where:

ΔP	Internal pressure
γ	Surface tension
σ	Charge density
D	Dielectric constant
ε_0	Permittivity of vaccum
r	Bubble radius

The internal gas pressure, ΔP, is estimated according to [Moleaer, n/aa] to be approximately 28.5 bar. This is considered in calculations in Section 2.5.1.

2.3 Documentation of nanobubbles

2.3.1 Method for generation of nanobubbles

There are many different methods to generate nanobubbles including:

- Cavitation
- Electrical
- Shear

Cavitation includes acoustic and hydrodynamic induced pressures change and nozzle based nanobubble generators [yu Zhang et al., 2020]. Ultra sound is an example of generating nanobubbles with cavitation [Bu and Alheshibri, 2021]. The external electrical method which uses electric fields is energy efficient and has high nanobubble densities [Wu et al., 2019]. Each method has its limitations and the choice of method will depend on the specific purpose and availability of equipment. The shear method is when gas is pushed through a membrane where there is a high liquid flow which then provides the shear force [Jadhav et al., 2021]. The gas enters the aqueous phase as dissolved gas as well as nanobubbles of which the dissolved gas is the largest fraction.

For this project a Lotus nanobubble generator from Moleaer was used [Moleaer, n/ab]. See section 2.4 for a description of the generators capacity as well as the experimental setup in this project. The Lotus unit use the shear method for generation of nanobubbles.

2.3.2 Measurement of oxygen content in nanobubble water

In order to determine the oxygen content in nanobubble water, Winkler titration experiments after the protocol of Abril et al. [2000, modified in 2007] have been conducted. The Winkler titration method to measure dissolved oxygen (DO) in waters was proposed in 1888 by chemist Lajos Winkler. Even though other methods have been developed for determining the dissolved oxygen content, e.g. membrane electrods, the Winkler method is still being used today.

Due to the stability of nanobubbles the oxygen content of nanobubbles is not dissolved in water. Hence a method to ensure the collapse of nanobubbles is necessary to measure the contained oxygen. Kikuchi et al. [2009] has presented a modified version of the traditional Winkler method. The modification made to the traditional Winkler method is that the

volume of the Winkler flask is filled with 1/5 water containing nanobubbles and 4/5 oxygen free water. Lastly, sulfuric acid is added to the flask, as the acid will burst the nanobubbles, and thereby increase the dissolved oxygen concentration.

For a more detailed description of both the Winkler method and the modified version, see Appendix A.

In addition to the Winkler experiments the oxygen release from nanobubbles was measured using an wireless fiber optic oxygen sensor [Loligo Systems, n/a]. Here the optic oxygen sensor measured the dissolved oxygen in the water. In order to compare the Winkler results there was also added 4/5 oxygen free water and 1/5 nanobubble water as well as acid in order to burst the nanobubbles. For more on this see Appendix B and Section 2.5.1.

2.3.3 Size distribution

In this project nanobubble water samples were analysed on a Zetasizer nano ZS. This is sufficient for size distributions in clean water but insufficient in terms of nanobubble concentrations [Malvern, April 2013].

According to Hashimoto et al. [2022] the concentration of nanobubbles in solution where the bubbles are being produced by the shear method is approximately $3.2 \cdot 10^8$ mL^{-1}.

The Zetasizer Nano ZS uses Dynamic Light Scattering (DLS) to estimate size distribution of particles. The Zetasizer registers the Brownian motions of the particles in the sample based on the light scatter created by the illuminated particles. This is utilised to determine the sizes of the nanobubbles [Malvern, April 2013].

The Zetasizer Nano ZS is a backscatter system where the laser is directed at the particles. The backscatter of the laser to determine the sizes of smaller particles in clean water [Meegoda et al., 2018]. The frontscatter method uses the same principles of the backscatter but detects the frontscatter of the light from the laser [Malvern, April 2013]. The backscatter system has been tested in comparision to forward scatter, more on this in section 2.5.2.

According to Moleaer [n/ac] the ideal instrument to determine the size of nanoparticles is a Nanoparticle Tracking Analysis (NTA). This is only ideal in clean water samples. The method also utilises the light scattering and Brownian motions as the DLS method. The major difference is that the NTA can also determines the concentration of nanobubbles in the sample.

2.3.4 Zeta potential

The Zetasizer Nano uses Electrophoretic Light Scattering technology to calculate the zeta potential [Malvern, April 2013].

The magnitude of the zeta potential gives an indication of the stability of the particle analysed. If the zeta potential exceeds a threshold of 30 mV - positive or negative - the particles are considered stable as they will tend to repel each other rather than flocculating [Malvern, April 2013]. Nanobubbles with a low zeta potential will be more unstable and the bubbles will tend to coalesce [Meegoda et al., 2018].

The zeta potential is dependant on pH-values. Therefore, it is important to note the zeta potential together with a pH-value, which in this project is approximately 7 [Malvern, April 2013]. For the precise values of pH see Appendix C and Excel sheet '1. Basic measurements'.

2.4 Experimental setup

For this project a Lotus nanobubble generator from Moleaer was used [Moleaer, n/ab]. The experimental setup for this project is shown in Figure 2.2 and 2.3. The setup consists of a nanobubble generator connected to a barrel with an approximate volume of 220 L. The gas inlet can be connected to O_2 (99.95%) or a compressor for atmospheric air (20.95%).

Figure 2.2. Experimental setup of the nanobubble generator.

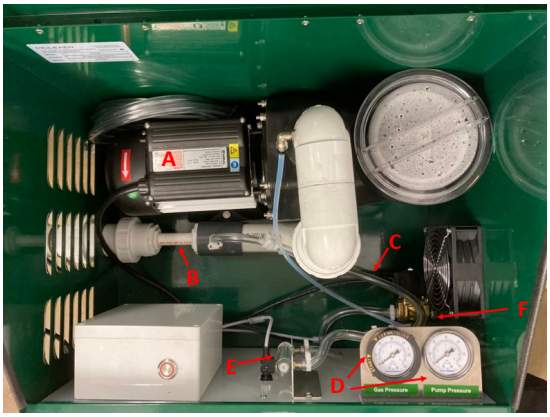

Figure 2.3. Experimental setup of the nanobubble generator. (A) pump, (B) membrane, (C) air hose, (D) pressure gauges, (E) rotameter and (F) gas inlet.

The nanobubble generator has a fixed water flow of 20 GMP equivalent to 75.7 L min^{-1}. This flow will only change as a result of resistance in the system. As Figure 2.2 shows the experimental setup does not have much resistance and it is therefore assumed that the water flow is at full capacity. For specifications of the Lotus unit see Appendix 'Lotus Owners Manual'.

The gas flow was tested at two different flows - 0.1 L min^{-1} and 0.05 L min^{-1} - and it was evident that this flow needed to be as small as possible to ensure the smallest bubbles. This can be seen in Appendix C and Excel sheet '1. Basic measurements'.

Table 2.1 shows the optimum setting for the nanobubble generator to ensure the best conditions for the smallest size distributions.

Table 2.1. The optimum settings for the nanobubble generator to ensure the most consistent results of nanobubbles.

Water pressure [bar]	**Water flow** [$L\ min^{-1}$]	**Gas pressure** [bar]	**Gas flow** [$L\ min^{-1}$]	**Volume** [L]	**O_2 delivery rate** [$mg\ L{\cdot}h^{-1}$]
∼1.2	∼75.7	∼0.9	∼0.05	220	7.55

There are four categories of measurements:

1. Demineralised water and atmospheric air
2. BOD water and atmospheric air
3. Demineralised water and oxygen
4. BOD water and oxygen

BOD water consists of demineralised water where solutions for BOD (biochemical oxygen demand) tests has been added. These solutions include: calcium chloride dihydrate (0.1 M), ferric chloride hexahydrate (0.9 mM), magnesium sulfate heptahydrate (0.09 M) and a phosphate buffer (0.1 M) [Cole-Parmer, n/a]. For calculations of amount added in order to make the solutions see Excel sheet '2. BOD solutions'.

The BOD water is used to ensure enough ion strength in relation to the Zetasizer and after suggestion from Moleaer making the experiments as representative to wastewater as possible [Moleaer, n/a]. This is evident when comparing results in demineralised water relative to demineralised water where BOD solutions have been added.

The starting point was demineralised water in combination with atmospheric air as atmospheric air is the most likely choice in a wastewater treatment plant. Since the measurement did not result in good data quality the lack of ions in the water was considered a possible explanation. Good data quality is based on measurement results on the Zetasizer. Therefore BOD solutions was added to the demineralised water. Although the analysis of the nanobubble samples subsequently resulted in better data quality and repeatability of results was still a challenge. According to Ushikubo et al. [2010] results with nanobubbles and oxygen give more stable results with good data quality and better repeatability. Therefore measurements with both demineralised water and BOD water and oxygen was tested. Here it was clear that the BOD water and oxygen yielded the best results in relation to repeatability and amount of measurements with good data quality.

2.5 Results of nanobubbles experiments

The following experiments are made in order to document the existence and formation of nanobubbles. The experiments made in this project are divided into three main categories: basic measurements, size distributions and zeta potential measurements.

2.5.1 Basic measurements

The basic measurements include measurements of dissolved oxygen content, temperature, redox potential, conductivity and pH. The basic measurements also include oxygen

measurements made with the modified Winkler tritration method as well as an optic oxygen sensor. See section 2.5.1.

Oxygen content

Figure 2.4 to 2.7 shows the oxygen content over time made in the four different categories as described in Section 2.5.1. The saturated oxygen level is based on temperature measurements during experiments. The temperature gennerally increases with time, as the water is circulated thought the pump and over the membrane approximately 30 times. The measured temperatures can be found in Appendix C. It can be seen that the dissolved oxygen exceeds saturated levels but this is achieved faster with oxygen than with atmospheric air. This applies for both demineralised water and BOD water. With atmospheric air the nanobubble generator has to run for a least 60 min before the dissolved oxygen level reaches saturation level, whereas with oxygen the generator has to run somewhere between 15 and 30 mins. Figure 2.6 and Figure 2.7 with oxygen nanobubbles bubbles only shows the oxygen content until 20 mg L^{-1} as this is the upper limit for the sensor used.

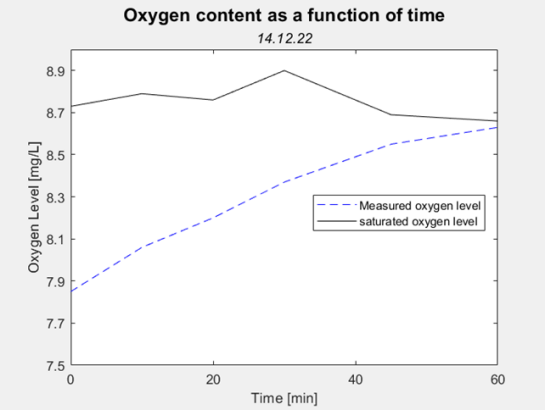

Figure 2.4. 14.12.22 - Dissolved oxygen as a function of time. Demineralised water and atmospheric air.

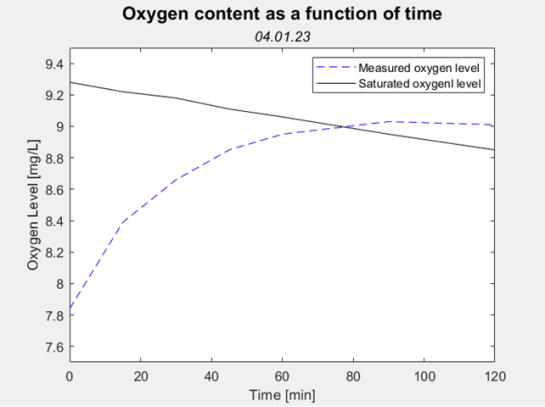

Figure 2.5. 04.01.23 - Dissolved oxygen as a function of time. BOD water and atmospheric air.

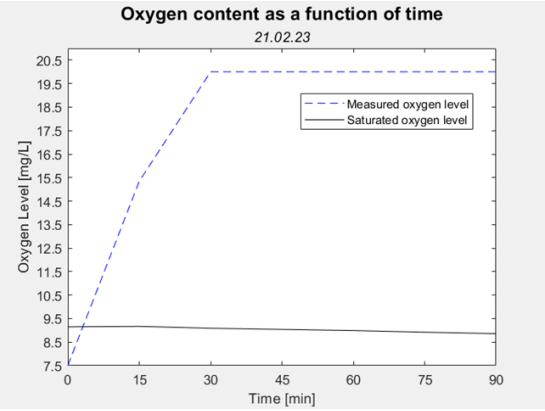

Figure 2.6. 21.02.23 - Dissolved oxygen as a function of time. Demineralised water and oxygen.

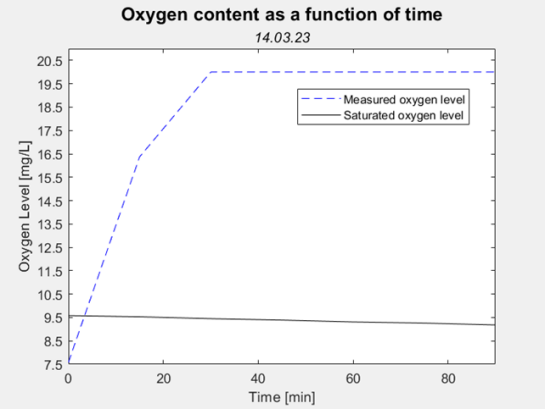

Figure 2.7. 14.03.23 - Dissolved oxygen as a function of time. BOD water and oxygen.

The redox potential was measured over time as well as the dissolved oxygen levels but as expected, the redox potential follows the oxygen content. For graphs of redox potential and measured oxygen content for the same days as Figure 2.4 to 2.7 see Appendix F. For graphs of redox potential for any other day see Excel sheet '1. Basic measurements'.

Winkler results

Table 2.2 shows the results of a modified Winkler titration made on 05.12.22. The results in the table are of nanobubbles with atmospheric air and in demineralised water. The nanobubble generator had run for 30 mins.

Table 2.2. Results of a modified Winkler titration to determine the oxygen content in nanobubbles. (DO) dissolved oxygen measured with an oxygen sensor after the nanobubble generator had run. No acid added. (DO after 2 days) dissolved oxygen level two days after the acid is added. (DO after 7 days) dissolved oxygen 7 days after the acid is added.

DO $[mg\,L^{-1}]$	**Temp.** $[°C]$	**Saturation** $[mg\,L^{-1}]$	**DO after 2 days** $[mg\,L^{-1}]$	**DO after 7 days** $[mg\,L^{-1}]$
8.45	22.1	8.73	10.01	11.65

As the table shows the acid added to lower the pH-value from ~ 7 to ~ 2 was added 2 and 7 days before the Winkler titration was done respectively. This was to see how long it would take for the acid to burst the nanobubbles. Although this experiment has not been repeated, it indicates an increasing trend in the concentration of dissolved oxygen. This could be because the oxygen content of the nanobubbles is released as the acid destabilises the nanobubbes and thereby increasing the dissolved oxygen level. The exact procedure for the method is described in Appendix A and the calculations can be found in Excel sheet '3. Winkler'.

The same experiment was performed using a optic oxygen sensor to ensure a continuous measurement of the dissolved oxygen level. The optic oxygen sensor experiments are made with the same conditions for water and gas as for the Winkler experiment, but these results shows that there is no increase in oxygen levels over time. This could be explained by the fact that the optic oxygen sensor measurement only had run for just over three hours. For the optic oxygen sensor results see Appendix B and Excel sheet '4. Optic oxygen sensor'.

In order to calculate the oxygen added to the water and the oxygen content in the nanobubbles, the Ideal Gas Law and Young la-place equations are used as well as a modified version of it, see Sections 2.2.2 and 2.2.1. The assumptions on which the calculations are based on can be seen in table 2.3. The concentration of 320 million nanobubbles pr. mL is based on literature as accounted in Section 2.3.3, since it was not possible to measure the concentration. The calculations for oxygen added to the water as well as oxygen content in the nanobubbles can be found in Excel sheet '5. Oxygen content nanobubbles'.

Table 2.3. Assumptions made to calculate the addition to the dissolved oxygen level as well as the oxygen content in the nanobubbles. The 2.25 L air added are based on an air flow of 0.05 L min^{-1} and a run time of the nanobubble generator for 45 mins. NB = nanobubbles.

Temp. $[^{\circ}K]$	**Gas constant** $[J/molK]$	**NB diameter** $[nm]$	**NB concentration** $[NB\,mL^{-1}]$	**Air added** $[L]$
292.15	8.31	270	320,000,000	2.25

Table 2.4 shows the results of the calculated oxygen content added to the water as well as the oxygen added to the nanobubbles. The oxygen added to the nanobubbles has been calculated using the conventional Young La-Place equation as well as the modified Young La-Place equation as described in Section 2.2.2.

Table 2.4. Estimation of oxygen added to the water phase (WP) and the nanobubbles (NB) from oxygen (O_2) or atmospheric air (A). *Modified Young La-place equation.

WP (O_2) $[mg\,L^{-1}]$	**WP (A)** $[mg\,L^{-1}]$	**O_2 NB** $[mg\,L^{-1}]$	**Pressure NB** $[bar]$	**O_2 NB*** $[mg\,L^{-1}]$	**Pressure NB*** $[bar]$
26.96	5.66	0.0005	11.79	0.0127	28.5

2.5.2 Size distributions of nanobubble samples

As mentioned earlier bubble size and zetapotential values were measured using a Malvern Zetasizer Nano Series ZS [Malvern, April 2013]. Similar to the basic measurements, size distributions were analysed every 15 minutes after the start of the nanobubble generator. Following a number of test runs there was a clear tendency that the best data quality and most consistent results were achieved 45 min after start of the nanobubble generator. This was where the bubble size was somewhat within acceptable range of the definition of nanobubbles i.e. 200 nm. For all the size distributions made see Excel sheet '6. Size distribution and zeta potential'.

The backscatter method is used based on literature found where the size of nanobubbles also are investigated [Meegoda et al., 2018]. As mentioned in Section 2.3.3 different settings were tested for the size distributions; backscatter and forward scatter as well as normal resolution and high resolution. Backscatter samples with both normal resolution and high resolution yields measurements with good data quality. However, fewer measurements were made using high resolution.

Table 2.5 shows the results of size distribution made with the different methods. The table shows which method is used, the average size distribution and standard deviation. Furthermore an interval of minimum and maximum size and how many measurements is of good data quality. If the analysis of the samples yielded measurements of good data quality a row is added below to show size data of good quality only. E.g. 29.03.23 there are 8 measurements out of 10 with good data quality, therefore there are made 2 rows from the 29.03.23 - one with values of all 10 measurements and one with values of the 8 good data quality measurements.

Table 2.5.(Quality) Number of measurement with good data quality out of the total number of measurement. If only one number is listed under the column 'quality', the numbers are averages for the measurements with good data quality. (FS NR) Forward scatter normal resolution, (FS HR) Front scatter high resolution, (BS NR) Back scatter normal resolution and (BS HR) Back scatter high resolution.

Date	**Method**	**Average size** $[nm]$	**Min. size** $[nm]$	**Max. size** $[nm]$	**Quality**
29/3-23	BS HR	206 ± 15	188	233	8/10
29/3-23	BS HR	208 ± 15	190	233	8
2/4-23	FS HR	335 ± 15	306	350	0/8
2/4-23	FS NR	388 ± 18	375	414	0/4
2/4-23	BS NR	251 ± 12	233	272	7
2/4-23	BS HR	258 ± 45	172	303	8/10
2/4-23	BS HR	253 ± 49	172	303	8

Table 2.6 shows all the size distribution samples. The nanobubble generator had run for 45 mins and the water passes the membrane approximately 15 times. All size distributions in the table are measured based on normal resolution.

Table 2.6. Size distribution measurements made after the nanobubble generator had run for 45 mins. (Quality) Number of measurement with good data quality out of the total number of measurement. If only one number is listed under the column 'quality' it means that the numbers are averages over the measurements with good quality. (D/A) Demineralised water and atmospheric air, (B/A) BOD water and atmospheric air, (D/O2) Demineralised water and oxygen, (B/O2) BOD water and oxygen and (T/A) Tap water and atmospheric air. *filtered sample.

Date	**Water/gas**	**Average size** $[nm]$	**Min. size** $[nm]$	**Max. size** $[nm]$	**Quality**
21/12-22	D/A	227 ± 43	181	318	0/10
4/1-23	B/A	$187. \pm 18$	156	215	1/10
4/1-23	B/A	175	-	-	1
5/1-23	B/A	181 ± 12	167	196	4/10
5/1-23	B/A	182 ± 14	167	196	4
9/1-23	B/A	369 ± 130	183	499	0/10
9/1-23	B/A	502 ± 79	349	582	0/10
10/1-23	B/A	362 ± 74	217	465	0/10
6/2-23	B/A	359 ± 46	310	430	7/10
6/2-23	B/A	366 ± 45	3010	430	7
8/2-23	B/A	434 ± 53	435	524	9/10
8/2-23	B/A	434 ± 53	435	524	9
10/2-23	T/A	282 ± 42	232	359	0/10
21/2-23	D/O2	351 ± 58	278	465	0/10
22/2-23	D/O2	215 ± 64	147	304	0/5
27/2-23	B/O2	479 ± 44	44	414	5/10
27/2-23	B/O2	475 ± 49	414	515	5
28/2-23	B/O2	291 ± 55	197	362	0/10
14/3-23	B/O2	459 ± 62	379	574	0/10
21/3-23	B/O2	292 ± 34	230	347	7/10
21/3-23	B/O2	291 ± 36	230	347	7
21-3-23*	B/O2	272 ± 12	254	286	5/10
21/3-23*	B/O2	277 ± 7	267	285	5
22/3-23	B/O2	268 ± 103	5	352	7/10
22/3-23	B/O2	256 ± 116	5	352	7
22/3-23*	B/O2	266 ± 15	249	277	0/3
29/3-23	B/O2	273 ± 24	221	312	9/10
29/3-23	B/O2	279 ± 17	258	312	9
26/4-23	B/O2	504 ± 96	392	651	0/10
26/4-23	B/O2	379 ± 86	252	507	2/10
26/4-23	B/O2	484 ± 32	461	507	2
12/5-23	B/O2	303 ± 11	284	316	0/10

It has been a time consuming process finding the optimum combination of gas and water yielding the data quality in terms of size distributions. As mentioned it was difficult to get good results and reproducing them in demineralised water. Hence the adjustments described in Section 2.5.1.

In demineralised water with atmospheric air (category 1) there was only 1 out of 10 samples

that had good data quality. For this sample the nanobubble generator had to run for 120 mins and the bubble size was approximately 250 nm.

As demineralised water was changed to BOD water (category 2). The basic measurement became more stable and easier to measure but the size distributions were still unstable as some days could give good data quality results but then the next time the generator ran with the same parameters, the size distributions had either no good data quality measurements or the average size was much larger than previous measurements. For example on the 09.01.23 where two samples were taken from the same batch after 45 min of nanobubble generator runtime.

Figure 2.8 to Figure 2.10 shows the graphs with good data quality made over three different days with the same parameters (category 4). This shows that there was three different days of measurements with good data quality which could be reproduced. The average size of the measurement with good data quality are 291 ± 36 nm for 21.03.23, 256 ± 116 nm for 22.03.23 and 279 ± 17 nm for 29.03.23. Based on the repeatability of the average size distribution these settings were used for the experiments made in Chapter 3 and Chapter 4.

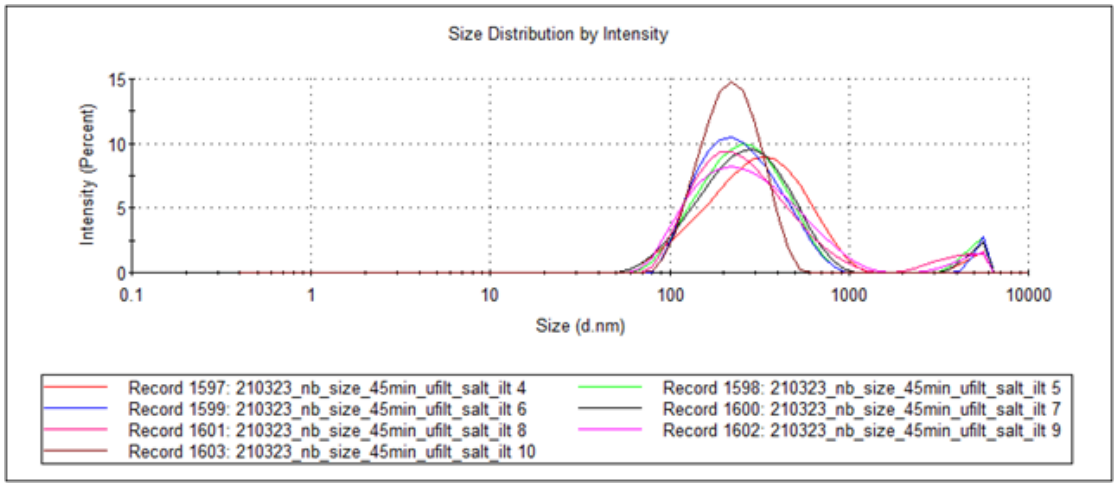

Figure 2.8.21.03.23. 7 out of 10 measurements with good data quality. The average size distribution is 291 ±36 nm.

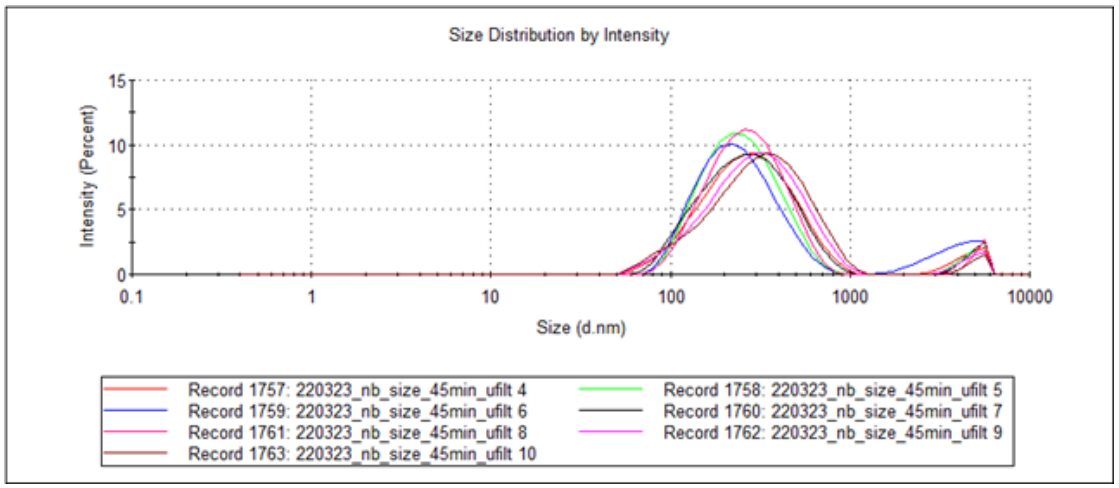

Figure 2.9.22.03.23. 7 out of 10 measurements with good data quality. The average size distribution is 256 ±116 nm.

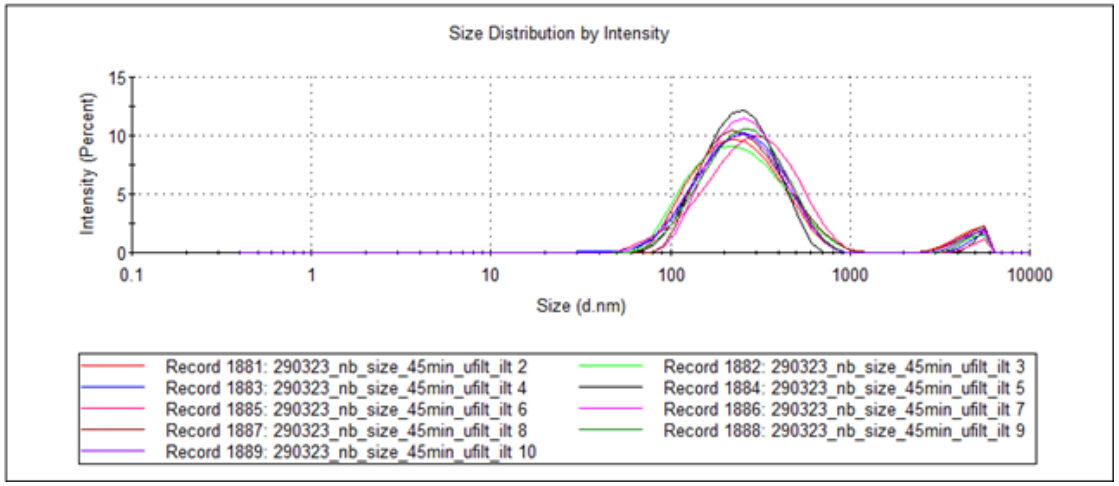

Figure 2.10.29.03.23. 9 out of 10 measurements with good data quality. The average size distribution is 278 ± 17 nm.

2.5.3 Zeta potential of nanobubble samples

Table 2.7 shows all data of the zeta potential measurements made after the nanobubble generator had run for 45 mins. Results from all four categories of water and gas type are included in the table.

As the Table 2.7 shows there is no good data quality for any of the zeta potential measurements. This includes measurements made at other times than 45 mins as well. Even though there is no good data quality there is still a clear tendency in the value of zeta potential at the different parameters. The zeta potential in BOD water and oxygen nanobubbles are approximately in an interval of -13 mV to -20 mV. See Excel sheet '6. Size distribution and zeta potential' for all zeta potential measurements.

Table 2.7.Zeta potential measurements made after the nanobubble generator had run for 45 mins. (Quality) Number of measurement with good data quality out of the total number of measurements. If only one number is listed under the column 'quality' it means that the numbers are averages over the measurements with good quality. (D/A) Demineralised water and atmospheric air, (B/A) BOD water and atmospheric air, (D/O2) Demineralised water and oxygen, (B/O2) BOD water and oxygen. *filtered sample.

Date	**Water/gas**	**Average zp** $[mV]$	**Min. size** $[mV]$	**Max. zp** $[mV]$	**Quality**
20/12-22	D/A	-12 ± 2	-16	-9	0/10
9/1-23	B/A	-17 ± 1	-19	-15	0/10
10/1-23	B/A	-17 ± 1	-19	-15	0/10
6/2-23	B/A	-14 ± 1	-16	-13	0/10
8/2-23	B/A	-15 ± 1	-17	-13	0/10
21/3-23	D/O2	-11 ± 3	-16	-7	0/10
22/3-23	D/O2	-10 ± 2	-13	-7	0/10
27/2-23	B/O2	-15 ± 2	-19	-12	0/10
28/2-23	B/O2	-18 ± 4	-25	-13	0/10
14/3-23	B/O2	-19 ± 1	-19	-17	0/10
21/3-23	B/O2	-20 ± 2	-23	-17	0/10
21/3-23*	B/O2	-2 ± 2	-6	-0.03	0/10
22/3-23	B/O2	-13 ± 1	-14	-11	0/10
22/3-23*	B/O2	-11 ± 1	-12	-8	0/10
2/4-23	B/O2	-16 ± 1	-18	-14	0/10

Table 2.8 shows the interval of the measured pH-values for the four categories. Without a buffer there is a tendency that the pH-value will decrease with time Moleaer [n/ac]. As a buffer is one of the BOD solutions the pH-values is much more stable and close to 7 as expected. See Excel sheet '1.Basic measurements' for all pH-values at every time step measured.

Table 2.8.The measured interval of pH-values of the four categories. (D/A) Demineralised water and atmospheric air, (D/O2) Demineralised water and oxygen, (B/A) BOD water and atmospheric air and (B/O2) BOD water and oxygen.

Water/gas	**Min pH-value**	**Max pH-value**	**Measurements**
D/A	5.3	7.7	3
D/O2	5.4	6.5	1
B/A	6.9	8.0	4
B/O2	7.1	7.5	4

Figure 2.11 shows the results of measurement made of the zeta potential at different pH-values. 10 measurement of zeta potential have been made at pH 2 to 9 and the showed value in the figure is an average of 10 measurements. See Excel sheet '7. Zeta potential vs pH' for all the data. The values for the zeta potential follows the same tendency of

increasing with increasing pH-values. This is the same tendency as experiments made in Meegoda et al. [2018]. Figure 2.11 also shows that at a pH-value below 3 the zeta potential becomes positive.

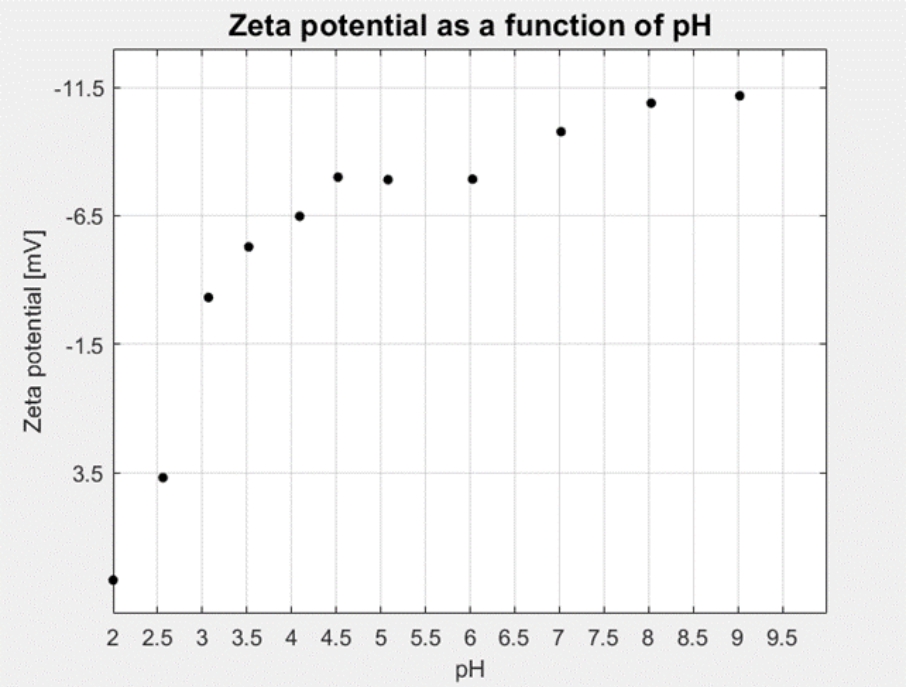

Figure 2.11.Zeta potential values at different pH-values. The measurements are made with nanobubble water after the generator had run for 45 mins.

3 Oxidative capacity of nanobubbles

As previously mentioned, nanobubbles potentially has a number of applications in water and wastewater treatment albeit these are not fully understood nor documented. In this project, the focus is on the oxidative capacity of nanobubbles. Having elaborated on the general properties of nanobubbles in Section 2 of the report, this section aims at elucidating the generation of reactive oxygen species (ROS) from nanobubbles. The process of generating ROS from nanobubbles is still debated. Firstly, it is still not clear whether ROS are generated at the interface between water and gas or if it requires the collapse of nanobubbles [Atkinson et al., 2019], see Figure 3.1. Secondly, Takahashi et al. [2017] and Soyluoglu et al. [2021] argues that the generation of ROS does not require a catalyst, while there is a general consensus that the formation of ROS can be achieved or accelerated from the destabilisation of nanobubbles by exposure to UV radiation, sonication or rapid pressure changes [Moleaer, n/ac], the addition of chemicals [Atkinson et al., 2019] or at a pH below 3 [Soyluoglu et al., 2021].

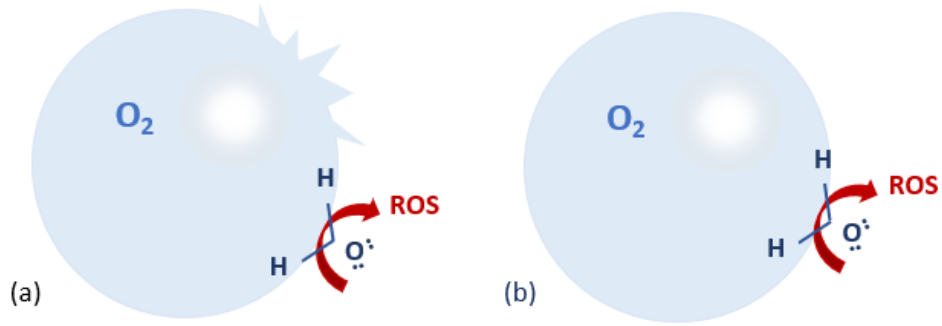

Figure 3.1.Different models for ROS generation (a) collapse of the nanobubbles (b) reaction at the gas-water interface. Modified from: [Atkinson et al., 2019].

Most publications concerning the generation of ROS are from the field of agriculture, while publications related to wastewater and nanobubbles generally have a focus on enhancement of biological processes e.g. by increasing oxygen availability. The aim of this study is to generate ROS from collapsing nanobubbles to oxidise APIs. In this project it is assumed that an exogenous source is necessary to destabilise the nanobubbles and generate ROS to achieve sufficient degradation.

3.1 Exogenous source of nanobubble collapse

Two exogenous sources to generate a collapse of nanobubbles have been suggested by Moleaer; sonication and UV light [Moleaer, n/ac]. The application of sonication requires high ultrasound frequencies; a study of ultrasound frequencies at 22 kHz, 43 kHz, 129 kHz, 488 kHz and 1 MHz found a decreasing trend in nanobubble concentration as the frequency increases, most notably for 488 kHz and 1 MHz [Yasuda et al., 2019]. However, different transducers were used for 22, 43 and 129 kHz than for 488 kHZ and 1 MHz. It adds to the complexity, that nanobubbles are generated at low frequencies at the optimum frequency of 22 kHz at 15 W according to Yasuda et al. [2019]. Numerous studies have investigated the generation of nanobubble using sonication [Bu and Alheshibri, 2021], [Yasuda et al., 2019], [Yasui et al., 2018] but little published material is available on sonication as a method of bursting nanobubbles.

UV radiation is already applied in water treatment internationally as disinfection as well as advanced oxidation processes [Collins and Bolton, 2016]. The UVC range from 200-280 nm is effective against bacteria and viruses and the range of most commercial UV units for advanced oxidation processes [Collins and Bolton, 2016]. Nanobubble exposure to shortwave UV is also known to generate ROS [Liu et al., 2016]. To test an exogenous source of nanobubble collapse that is easily scaleable, UV light at a wavelength of 254 nm is chosen for the experimental setup described further in Section 3.3.

3.2 Reactive oxygen species

Liu et al. [2016] studied the formation of ROS from nanobubbles and sought to distinguish between superoxide anion radicals, hydrogen peroxide, hydroxyl radicals and singlet oxygen. A flourescent probe (3'-p-(aminophenyl) fluorescein) (APF) was used to detect and distinguish between ROS as these have different flourescent responses. It was demonstrated that the ROS generated from nanobubbles is $^{\cdot}OH$.

The hydroxyl radicals are relevant, due to the high standard reduction potential relative to other oxidants as shown in Table 3.1. Hence, if hydroxyl radicals are generated from the destabilisation of nanobubbles these could theoretically prove efficient in the degradation of APIs.

Table 3.1. The standard reduction potential of hydroxyl radicals relative to other oxidising agents [Weast, 1977].

Oxidising agent		**Standard reduction potential E^o** $[V]$
Hydroxyl radical	$^{\cdot}OH$	2.80
Ozone	O_3	2.07
Hydrogen peroxide	H_2O_2	1.77

3.2.1 Hydroxyl radical indicators

Hydroxyl radicals cannot be measured directly, hence an indicator is necessary. In a addition to the flourescent probe (3'-p-(aminophenyl) fluorescein) applied by Liu et al. [2016], Michailidi et al. [2020] and Takahashi et al. [2017] made use of electron-spin resonance. Satoh et al. [2007] tests methylene blue due to the simplicity of the method and verifies the method using benzoic acid and thin-layer chromatography. These methods have all been tested in combination with a Fenton reation, see Section 3.2.2. However, the methylene blue has also been applied as an indicator of hydroxyl radical formation by Moleaer [Moleaer, n/a] as well as Minamoto et al. [2021]. Two methods are explored further; methylene blue and benzoic acid in Section 3.2.4 and 3.2.3 respectively.

3.2.2 Fenton's reaction

To test the application of ·OH indicators, controlled formation of ·OH is necessary. The Fenton reaction is a widely approved method for this purpose [Harris and Lucy, 2019] and has also been applied in studies of ROS in relation to nanobubbles [Liu et al., 2016]. The Fenton reaction as given in Equation 3.1 is the oxidation of iron(II) and reduction of hydrogen peroxide to form iron(III), hydroxide and hydroxyl radicals.

$$Fe^{2+} + H_2O_2 \rightarrow Fe^{3+} + OH^- + OH^{\cdot} \tag{3.1}$$

The reation efficiency depends on pH as well as the molar ratio of iron(II) and hydrogen peroxide [Satoh et al., 2007]. Two combinations of molarities and molar ratios were tested as given in Table 3.2. Both references made use of the Fenton reaction to degrade methylene blue.

Table 3.2. Overview of Fenton reactions tested for the generation of hydroxyl radicals and which indicators were tested. (MB) Metyhlene blue. (BA) Benzoic acid.

Molar ratio	**Molarity Fe^{2+}**	**Molarity H_2O_2**	**pH**	**pH adjusted**	**Indicator**	**Reference**
1:20	0.15 mM	3 mM	3	H_2SO_4	MB BA	[Satoh et al., 2007]
1:4	2 mM	8 mM	3	HCl	MB	[Melgoza et al., 2009]

A detailed description of the Fenton experiments can be found in Appendix D.

3.2.3 Benzoic acid

Benzoic acid can be applied as an indicator of hydroxyl radicals, and the formed complexes will be detectable using spectrophotometry at wavelength 517 nm [Satoh et al., 2007]. Satoh et al. [2007] added finely ground benzoic acid to a Fenton reaction to achieve a final benzoic acid concentration of 9 mM. As the solubility of benzoic acid in water is only 3.5 g L^{-1}, the benzoic acid is only gradually dissolved, and as a result hydroxyl radical degradation of benzoic acid is only gradual.

The Fenton's reaction was initially tested using benzoic acid, but the formed iron complexes detectable at wavelength 517 nm are only formed under acidic conditions and requires iron(II) in the solution [Satoh et al., 2007; da Silva et al., 1998]. Hence this method was not explored further, as acidic conditions are not compatible with nanobubble samples i.e. nanobubbles collapse. Furthermore, benzoic acid has two absorbance peaks between 200 and 300 nm, but due to the low solubility of benzoic acid in water, there will be no baseline for the absorbance. Details on preliminary testing of benzoic acid, can be found in Appendix D.

3.2.4 Methylene blue

Methylene blue is a dye used for e.g. textiles. In the reaction of the methylene blue cation and hydroxyl radicals, a colourless methylene blue radical cation is formed instead [Satoh et al., 2007]. This makes methylene blue a potential indicator of hydroxyl radicals.

Methylene blue can be detected by spectroscopi and has a peak absorbance at 665 nm [Melgoza et al., 2009]. Two additional peaks can be measured for methylene blue at wavelengths 250 nm and 300 nm [Melgoza et al., 2009]. These are however not considered in this project based on [Melgoza et al., 2009]. In addition it was decided to use polystyrene cuvettes to avoid discolouration of a quartz cuvette, but polystyrene cuvettes do not allow for measurements at 250 nm or 300 nm. In studies of methylene blue degradation, the concentrations investigated varies significantly. Referring back to the Fenton reactions in Table 3.2, the concentration of methylene blue was 1 mM [Satoh et al., 2007] and 0.16 mM [Melgoza et al., 2009] respectively. A literature search yielded no results for the degradation of methylene blue as a result hydroxyl radicals from nanobubbles. For this reason a concentration of 0.16 mM was chosen for methylene blue tests in this study, as this is the methylene blue concentration that corresponds to the reference chosen for the Fenton reaction [Melgoza et al., 2009]. After the conclusion of the final tests, input was received from Moleaer that good results had been achieved in nanobubble tests at a methylene blue concentration of $0.3 \cdot 10^{-3}$ mM i.e. a significantly lower molarity than in the studies of the Fenton reaction [Moleaer, n/a].

3.3 Experimental setup

Two experimental setups were tested; (1) a peristaltic pump generating a flow between the methylene blue sample and a UV_{254} chamber and (2) circulation (magnetic stirring) in a beaker containing the methylene blue sample as well as a submerged UV_{254} bulb. Experimental setup 1 is shown in Figure 3.2. The circulated volume was initially 200 mL.

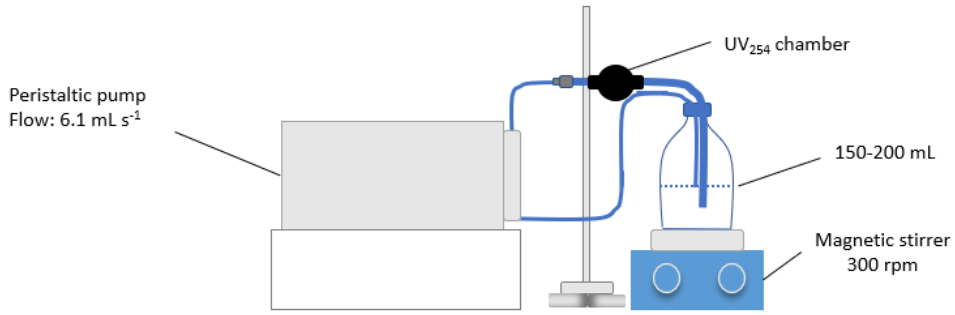

Figure 3.2.Experimental setup 1. A 0.16 mM methylene blue sample is circulated by a peristaltic pump from a 250 mL bluecap bottle to a UV_{254} chamber and via the pump back to the bluecap bottle.

Due to feedback on initial results the setup was altered to experimental setup 2 as shown in Figure 3.3 in an attempt to ensure greater exposure of the sample to the UV light. The sample volume had to balance the smallest possible volume, but at the same keep the bulb submerged in the solution while continuously sampling every 15 minutes for an hour.

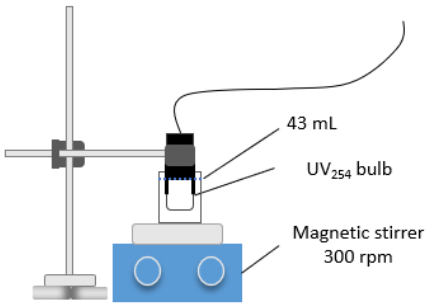

Figure 3.3.Experimental setup 2. A 0.16 mM methylene blue sample is stirred in 50 mL beaker. The UV_{254} bulb is submerged in an volume of 43 mL prior to sampling. The beaker and bulb covered in aluminum foil while the UV bulb is on.

The change in experimental setup yielded no improvement in methylene blue degradation rate, hence the experimental setup was changed back to experimental setup 1 and the circulated volume was decreased from 200 mL to 150 mL to optimise retention time in the UV chamber. It was not possible to reduce the volume further due to continuous sampling. The flow had already been reduced to a minimum to ensure circulation in the system setup. Experimental setup 1 was used for methylene blue degradation experiments as well as for the degradation of APIs described in Chapter 4.

Four scenarios are tested:

1. Circulation only (BOD solution)
2. UV_{254} light (BOD solution)
3. A nanobubble sample
4. A nanobubble sample and UV_{254} light

3.4 Results

3.4.1 Fenton reaction

The Fenton reaction degradation of methylene blue was tested as well as effects of iron(II)sulfate, hydrogen peroxide and a sample of methylene blue only. For each of these three components as well as the Fenton reaction the absorbance was measured at 0 minutes and 5 minutes. The 0 minute sample for the Fenton reaction was sampled immediately after adding the hydrogen peroxide to the iron(II)solution. After five minutes, no degradation of methylene blue was registered for the samples containing methylene blue only, iron(II) or hydrogen peroxide. All methylene blue was degraded by the Fenton reaction.

This result indicates that methylene blue can be used as an indicator of hydroxyl radicals, as it is clear that it is the hydroxyl radicals from the Fenton reaction that degraded the methylene blue. For more results see Appendix D.

3.4.2 Methylene blue degradation

A methylene blue sample was analysed using spectrophotometry every 15 minutes for a total of 60 minutes. For each experiment, the variation in absorbance in one time step was up to 17%. Although the trendlines for the combination of nanobubbles and UV for 150 mL samples all have negative coefficients - unlike the results from other experiment combinations - there was no consistency in results. The coefficients of determination are generally ranging between 0 and 0.25. Trends from 0-60 minutes for all methylene blue experiments as well as coefficients of determination are presented in Table 3.3. For the sample volumes 150 mL and 200 mL experimental setup 1 in Figure 3.2 was used and for the sample volume of 43 mL, experimental setup 2 in Figure 3.3 was used.

Table 3.3. Trends from 0-60 minutes and coefficient of determination for the degradation of methylene blue testing (1) Circulation only, (2) UV light (3) a nanobubble sample and (4) a nanobubble sample combined with UV. The methylene blue concentration is 0.05 g L^{-1} in all experiments.

Sample volume $[mL]$	**Coefficient**	**R^2**	**Sample volume** $[mL]$	**Coefficient**	**R^2**
Circulation:			UV:		
150	$-0.3 \cdot 10^{-3}$	> 0.1	43	$-0.3 \cdot 10^{-3}$	> 0.1
150	$0.4 \cdot 10^{-4}$	> 0.1	43	$-0.8 \cdot 10^{-3}$	0.23
200	$-0.2 \cdot 10^{-3}$	> 0.1	43	$0.2 \cdot 10^{-3}$	> 0.1
200	$-0.6 \cdot 10^{-3}$	0.15	150	$-0.9 \cdot 10^{-3}$	> 0.1
200	$0.2 \cdot 10^{-3}$	> 0.1	150	$0.1 \cdot 10^{-4}$	> 0.1
			200	$-0.2 \cdot 10^{-3}$	> 0.1
			200	$-0.1 \cdot 10^{-3}$	> 0.1
			200	$0.3 \cdot 10^{-3}$	> 0.1
Nanobubbles:			Nanobubbles and UV:		
150	$-1.0 \cdot 10^{-3}$	0.15	43	$-1.0 \cdot 10^{-3}$	0.11
150	$-1.0 \cdot 10^{-3}$	0.20	43	$0.5 \cdot 10^{-3}$	> 0.1
			43	$0.5 \cdot 10^{-3}$	> 0.1
			150	$-3.0 \cdot 10^{-3}$	0.69
			150	$-2.0 \cdot 10^{-3}$	0,25
			150	$-1.0 \cdot 10^{-3}$	> 0.1
			150	$-0.9 \cdot 10^{-3}$	0.16
			200	$-3.0 \cdot 10^{-3}$	0.49
			200	$-1.0 \cdot 10^{-3}$	0.25
			200	$0.1 \cdot 10^{-3}$	> 0.1
			200	$0.1 \cdot 10^{-3}$	> 0.1
			200	$0.4 \cdot 10^{-3}$	> 0.1
			200	$0.9 \cdot 10^{-3}$	0.13

The highest coefficient of determination was 0.69 achieved for the combination of nanobubbles and UV showing a trendline coefficient of -0.003. A plot of these data can be seen in Figure 3.4. Even considering outliers, the result indicates that methylene blue is degraded in this one experiment. However, this result must be considered an outlier as it was not possible to repeat this. Figure 3.5 is a more representative plot where the decrease in absorbance is not consistent and the outliers from timestep 0 min. and 60 min. overlap. All plots can be found in Excel sheet '8. Methylene blue experiments'.

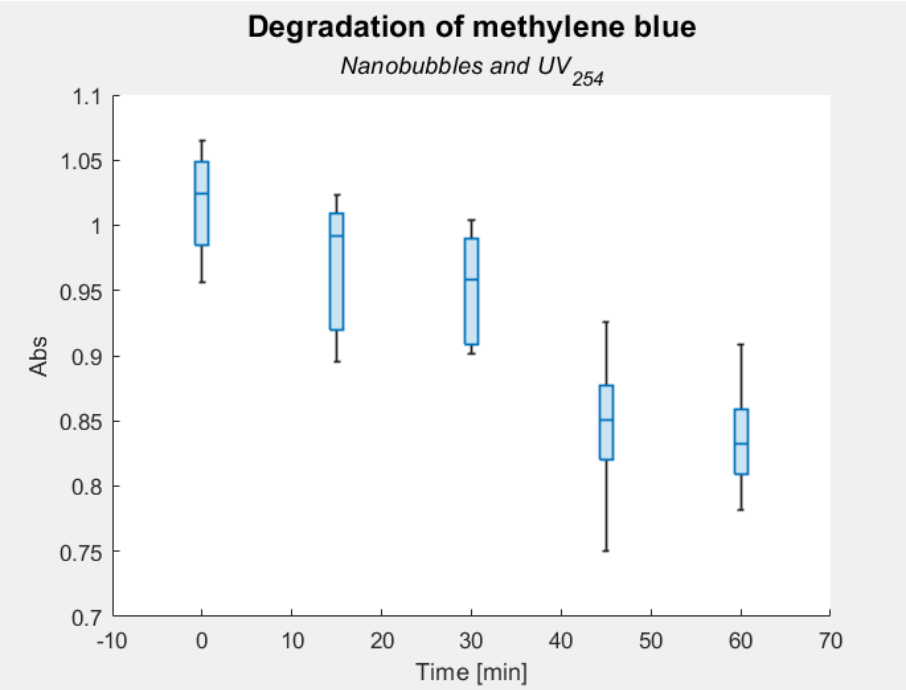

Figure 3.4. Degradation of methylene blue as a function of time in a 150 mL sample. R^2 is 0.69.

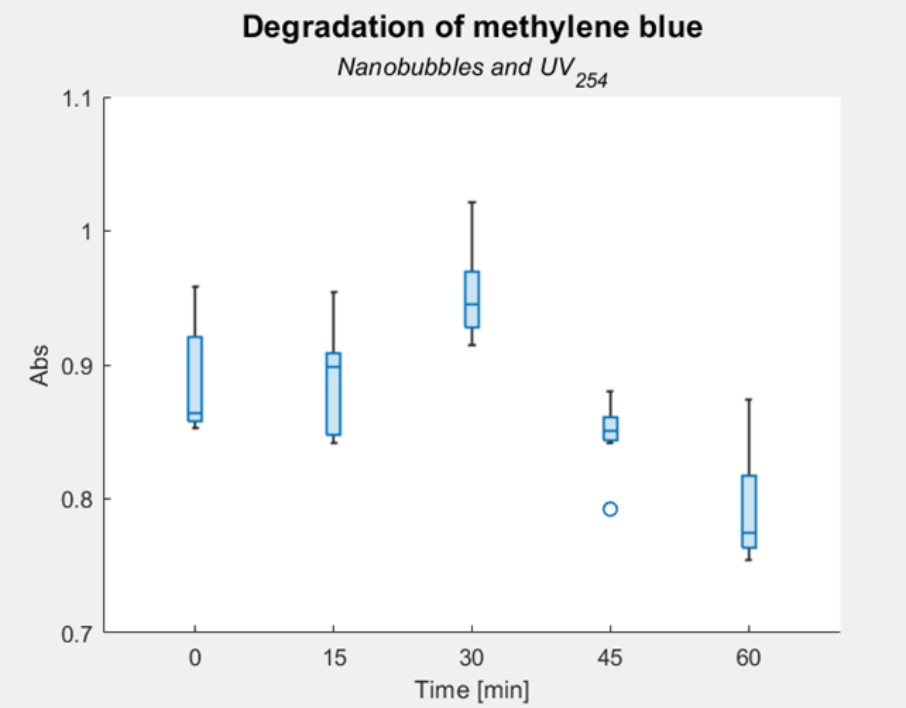

Figure 3.5. Degradation of methylene blue as a function of time in a 150 mL sample. R^2 is 0.25.

4 Degradation of active pharmaceutical ingredients

In Chapter 3, no significant degradation of methylene blue was detected based on the method of generation and settings accounted for in Chapter 2. In this section, the aim is to investigate whether the synergy of nanobubbles and UV can be utilised to degrade API concentrations by oxidation. For this analysis two APIs was selected; diclofenc and venlafaxine. Diclofenac is an analgesic and anti-inflammatory pharmaceutical whereas venlafaxine is used for treatment of disorders related to the nervous system e.g. depression or anxiety.

Diclofenac experiments were conducted first, as this is easily degraded by oxidation processes [Jensen et al., 2022]. On the basis of results that will be presented in Section 4.4 a decision was made that the API for the following experiments should be more difficult to degrade using oxidation processes as well as UV light [Drastrup, 2022; Ikonen et al., 2021].

4.1 APIs in wastewater effluents

This report has a focus on APIs found in the effluent of Danish wastewater treatment plants i.e. substances that are not degraded by mechanical or conventional activated sludge treatment. The removal efficiency of diclofenac in a conventional activated sludge treatment process has been found to be below 40% in five Danish wastewater treatment plants [Jensen et al., 2022; The Danish Environmental Protection Agency, 2022; Bailon et al., 2021]. Venlafaxine often has negative removal rates [Jensen et al., 2022; The Danish Environmental Protection Agency, 2022; Bailon et al., 2021]. Diclofenac and venlafaxine are included in this study on the basis of two main criteria:

- The concentration exceeds PNEC in the effluent of more than one Danish wastewater treatment plant
- Is included in the list of APIs targeted in the proposal for a Directive concerning urban wastewater treatment

The Danish Water and Wastewater Association (DANVA) has published a report, where the effluent from ten Danish wastewater treament plants was analysed [DANVA, 2021]. Diclofenac as well as venlafaxine was detected in the effluent from all ten wastewater treatment plants included in the study. Only diclofenac is detected in Danish streams [Naturstyrelsen, 2015], but this may be because only specific APIs included in the

NOVANA programme. Venlafaxine is one of the substances suggested for the EU watch list, and may as a result be included in NOVANA [Loos et al., 2018].

4.2 Classification of risk related to APIs

APIs may be problematic in terms of public health if found in drinking water resources. As a result, Switzerland has introduced legislation aimed at reducing the discharge concentration of twelve selected xenobiotics including diclofenac and venlafaxine [DANVA, 2021]. In Denmark where drinking water is extracted from groundwater, the attention has been directed more towards the health risks posed by pesticides and PFAS, but little has been documented in relation APIs in groundwater [Stuer-Lauridsen et al., n/a]. This could be relevant as wastewater sludge is used as fertiliser in Denmark. In addition to public health concerns APIs has a documented effect on aquatic environments. Diclofenac is categorised as acute toxic (oral) at doses above 50 mg kg $^{-1}$ and causes renal effect as well as impact on liver and the gastrointestinal system in humans [Cuklev et al., 2011]. Diclofenac also has similar adverse effects in fish in particular at concentrations as low as 1 μg L^{-1}, but cell necrosis in gills has also been observed [Cuklev et al., 2011]. Venlafaxine is not toxic to humans but there are indications that the substance causes behavioral effects in fish e.g. predation ability [Jr et al., 2014; Maulvault et al., 2018].

The Ministry of Environment in Denmark approaches risk assessment using an A-B-C classification [Miljøministeriet, 2018]. These are elaborated in an instruction from the Environmental Protection Agency and briefly described below [Miljøstyrelsen, 2006].

- **A** Substances that should not be found in wastewater due to high toxicity to humans or aquatic organisms and are difficult to degrade

- **B** Substances that should meet the set environmental quality standards. These substances are not toxic to humans, but has a medium toxicity to aquatic organisms, may bioaccumulate or is difficult to degrade

- **C** Substances that are not included categories A and B i.e. they are not toxic or difficult to degrade and they do not bioaccumulate

This instruction also includes a list of specific substances and suggestions for environmental quality standards for group B classified substances. Diclofenac and venlafaxine are not included on this list, but it is also worth mentioning that it has not been updated since 2006.

DHI - a consultancy and research organisation in the field of water environment - published a report in 2013 that should serve as guideline for the municipal regulation of hospital wastewater [DHI, 2013]. At this point in time APIs was a focus of the Ministry of Environment of Denmark as well as the municipalities, which may be a result of the centralisation of the secondary health sector mentioned in the introduction. In this report by DHI diclofenac and venlafaxine are listed as category A and category C substances respectively [DHI, 2013]. However, in a more recent assessment of Odense University hospital (OUH) from 2021 venlafaxine is listed as a category B substance [DHI and EKJ, 2021].

4.2.1 Risk assessment

A number of parameters can be utilised to describe the risks APIs pose to health and environment. A common measure of the concentration limit for adverse effects is PNEC. This is a measure of the maximum concentration of a substance to ensure the set environmental quality standards are met. Another indicator is the octanol water partitioning coefficient often expressed as $\log K_{ow}$. This is an indicator of the tendency of a substance to bioaccumulate [DHI, 2013]. The classification as well as the indicators PNEC and $\log K_{ow}$ are given for diclofenac and venlafaxine in Table 4.1.

Table 4.1. The risk classification of diclofenac and venlafaxine as well as the indicators PNEC and $\log K_{ow}$. 1) [DHI and EKJ, 2021], 2) [Loos et al., 2018], 3) [DHI, 2013]

	Classification [1)]	**PNEC** [2)] $[\mu g\ L^{-1}]$	**logK_{ow}** [3)] [-]
Diclofenac	A	0.050	3.90
Venlafaxine	B	0.038	0.43

The PNEC values for diclofenac and venlafaxine presented in the table are updated values from the EU Watch list [Loos et al., 2018]. The ratio between PEC (Predicted Environmental concentration) and PNEC is an indicator of risk and generally a PEC/PNEC > 1 indicates indicates an environmental risk [DHI, 2013]. However, PEC may fluctuate during the year as a result of variations in the consumption of APIs during the year as well as the dilution factor in the recipient [Miljøstyrelsen, 1998]. In Table 4.1 the presented $\log K_{ow}$ clearly indicates why diclofenac bioaccumulates and cause adverse effects in liver and kidneys, as a $\log K_{ow} > 1$ indicates a lipophilic substance and a tendency to accumulate in fatty tissue.

4.3 Experimental account

The experimental setup for degradation of diclofenac end venlafaxine is the same as for the degradation of methylene blue as illustrated in Figure 3.2. To separate the effects of nanobubbles, UV and nanobubbles, the same four categories were used for the API experiments as for the methylene blue described in Section 3.3. For experiments in this section samples were analysed every 10 minutes, rather than every 15 minutes as was the case for the methylene blue experiments. This adjustment was made to better be able to estimate whether the degradation rate is lineary or exponential.

Diclofenac sodium salt was used for the diclofenac experiments as this is more soluble in water and venlafaxine hydrochloride was used for the venlafaxine experiments [pro.medicin.dk, 2023], see Table 4.2.

Table 4.2.CAS number, empirical formula and molecular weight of diclofenac sodium and venlafaxine hydrochoride.

	Empirical formula	**Molar weight** $[g\ mol^{-1}]$	**CAS number**
Diclofenac sodium salt	$C_{14}H_{10}Cl_2NNaO_2$	318.13	15307-79-6
Venlafaxine hydrochloride	$C_{17}H_{27}NO_2{\cdot}HCl$	313.86	99300-78-4

The chemical structure of the compounds is shown in Appendix G.

4.3.1 HPLC

Samples were analysed using reverse phase UV HPLC (high-performance liquid chromatography). For both diclofenac and venlafaxine, gradient elution was used. An overview of HPLC specifics for each API is presented in Table 4.3.

Table 4.3.HPLC settings for diclofenac sodium salt and venlafaxine hydrochoride.

	Diclofenac sodium	**Venlafaxine**
Concentration $[g\ L^{-1}]$	0.1	0.1
Eluents	Acetonitrile/2% Phosporic acid	Methanol/KH_2PO_4
Injection volume [μL]	20	50
Flow [mL min^{-1}]	1	1
Run time [min.]	15	15
UV wavelength [nm]	276	226

Diclofenac sodium salt

Previous studies was the basis of the concentrations and HPLC programmes used for the analysis in this Chapter, but particularly for diclofenac sodium, there were numerous combinations of eluents. Hence, a number of adjustments were made to this HPLC programme, but the starting point for the eluent was acetonitrile [Soheili-Azad et al., 2020]. During the first 5 minutes of the programme the initial ratio of acetonitrile/phosphoric acid was 50/50%. After five minutes acetonitrile was increased linearly to 100/0% at 15 minutes. The UV HPLC limit of quantification for sodium diclofenac was found to be in the range 0.24-1.75 μg L^{-1} in a review by Soheili-Azad et al. [2020].

Venlafaxine hydrochlorid

The HPLC programme for venlafaxine hydrochloride was made on the basis of Ewelina Dziurkowska [2013]. The initial ratio of methanol/phosphate buffer was 40/30% for the first five minutes with a linear increase in methanol to methanol/phosphate buffer 70/30% between 5 and 15 minutes. The HPLC limit of quantification for venlafaxine hydrochloride is approximately 5-10 μg L^{-1} [Raut et al., 2003; Ewelina Dziurkowska, 2013].

4.4 Results

A standard curve was made for both APIs which show a linear tendency. See Appendix E for the standard curves of diclofenac and venlafaxine.

4.4.1 Diclofenac

Figure 4.1 to 4.6 shows the graphs of the degradation rate of diclofenac for the four categories introduced in Section 3.3. As Figure 4.1 and Figure 4.2 shows there is no correlation for the data in these experiments and therefore it is not possible to make a fit for the curves. Figure 4.3 and 4.4 as well as Figure 4.5 and 4.6 shows a second order degradation rate and a coefficient of determination of 0.99.

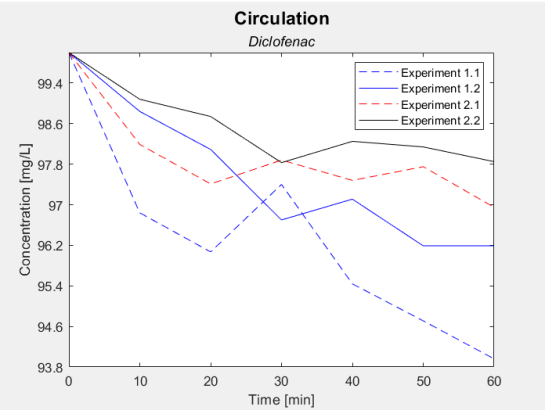

Figure 4.1. Hourly degradation of diclofenac with circulation. There is no clear trend in the distribution of data.

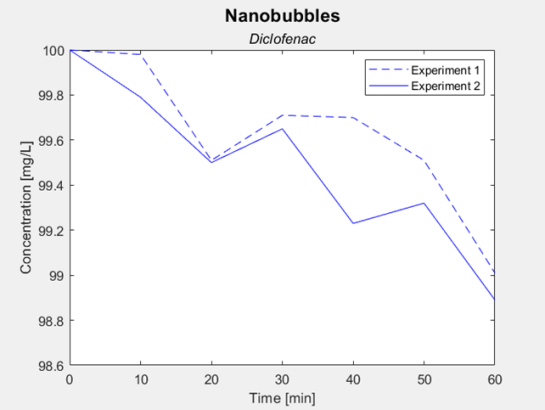

Figure 4.2. Hourly degradation of diclofenac with nanobubbles. There is no clear trend in the distribution of data.

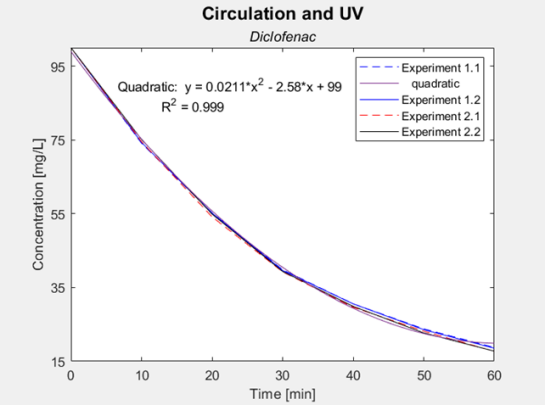

Figure 4.3. Hourly degradation of diclofenac with circulation and UV. The purple fitted line is for experiment 1.1.

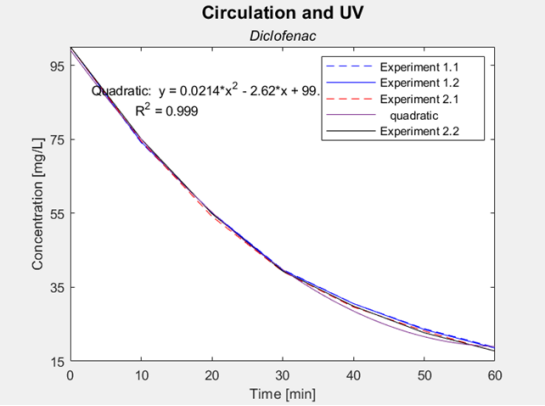

Figure 4.4. Hourly degradation of diclofenac with circulation and UV. The purple fitted line is for experiment 2.1.

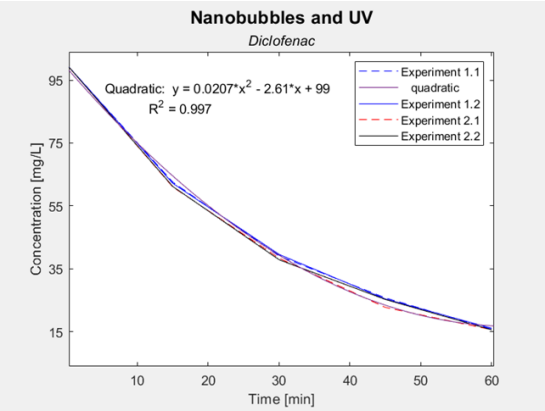

Figure 4.5. Hourly degradation of diclofenac with nanobubbles and UV. The purple fitted line is for experiment 1.1.

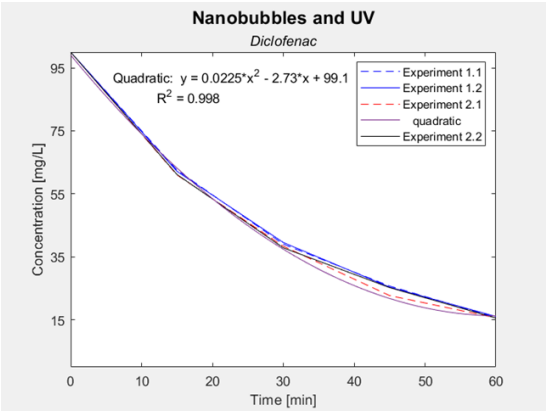

Figure 4.6. Hourly degradation of diclofenac with nanobubbles and UV. The purple fitted line is for experiment 2.1.

Table 4.4 shows the average removal efficiency for diclofenac for one hour in the four categories as well as an interval of minimum and maximum degradation efficiencies. The results shows that the primary factor contributing to the degradation of diclofenac is the UV light. There is a higher degradation rate when combining UV and nanobubbles compared to UV light alone as the average removal rate increases from 81.82 % to 84.66 %.

Table 4.4. The average removal efficiency over an hour for diclofenac. For calculations see Excel sheet '9. Pharmaceutical experiments'.

	Avg. removal efficiency [%]	**Minimum** [%]	**Maximum** [%]	**Experiments**
Circulation	3.77	2.15	6.04	4
Circulation + UV	81.82	81.26	82.31	4
Nanobubbles	1.05	0.99	1.11	2
Nanobubbles + UV	84.66	83.92	85.53	7

4.4.2 Venlafaxine

Figure 4.7 to 4.12 shows the graphs of the degradation in one hour for venlafaxine. Figure 4.9 and Figure 4.10 shows a low coefficient of determination for the experiments and the concentration over time actually increases from 40 min to 50 min even though the overall tendency is decreasing. The combination of nanobubbles and UV light shown in Figures 4.11 and 4.12 has the best linear fit as the coefficients of determination are 0.987 and 0.998.

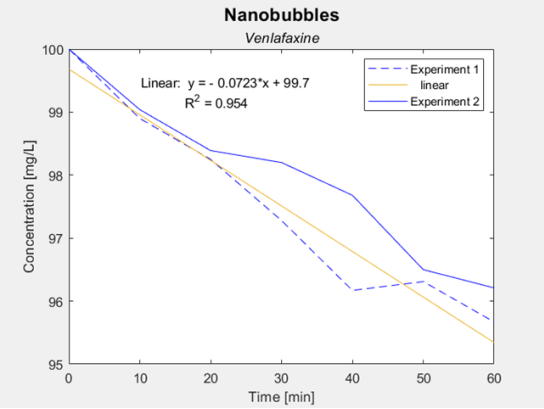

Figure 4.7.Hourly degradation of venlafaxine with nanobubbles. The yellow linear fitted line is for experiment 1.

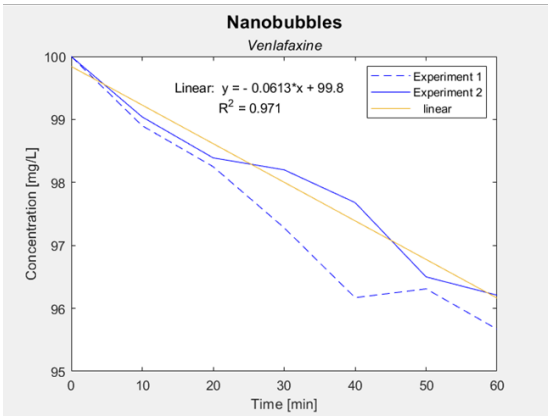

Figure 4.8.Hourly degradation of venlafaxine with nanobubbles. The yellow linear fitted line is for experiment 2.

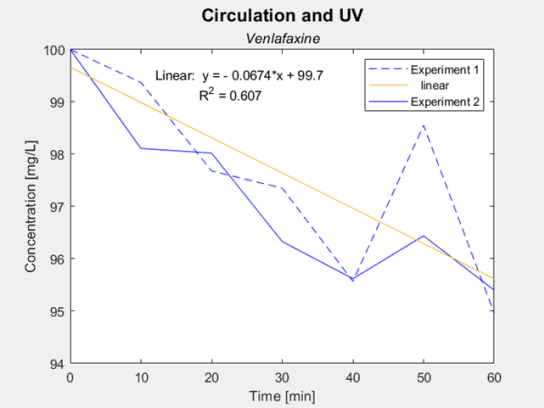

Figure 4.9.Hourly degradation of venlafaxine with circulation and UV. The yellow linear fitted line is for experiment 1.

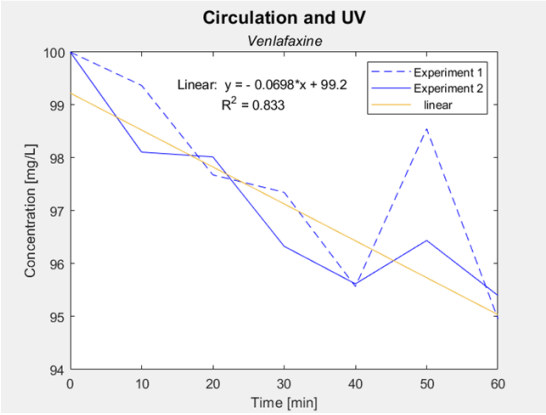

Figure 4.10.Hourly degradation of venlafaxine with circulation and UV. The yellow linear fitted line is for experiment 2.

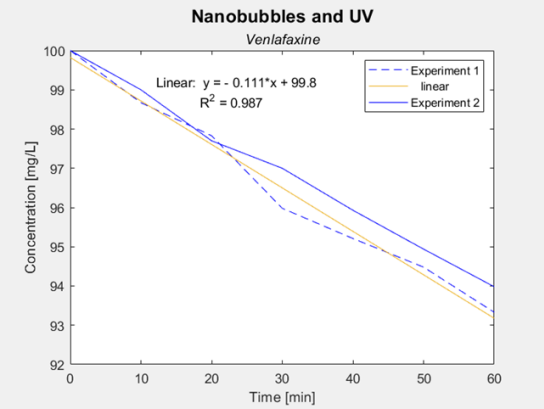

Figure 4.11.Hourly degradation of venlafaxine with nanobubbles and UV. The yellow linear fitted line is for experiment 1.

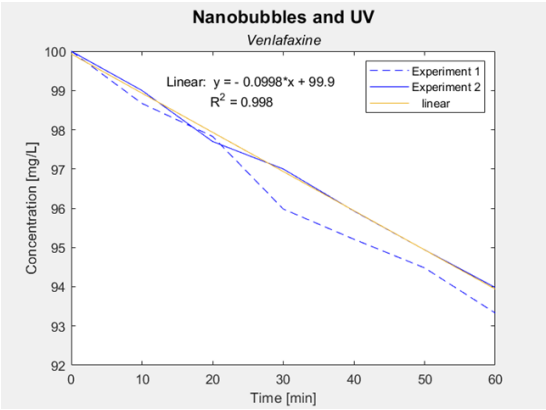

Figure 4.12.Hourly degradation of venlafaxine with nanobubbles and UV. The yellow linear fitted line is for experiment 2.

Table 4.5 shows the average degradation of venlafaxine in one hour for the three categories as well as an interval of minimum and maximum degradation. These degradation rates show that there is an increase in degradation when combining nanobubbles with the UV light compared to UV light and circulation or nanobubbles. The overall degradation rate is not as effective for venlafaxine as for diclofenac.

Table 4.5. The average removal efficiency over an hour for venlafaxine. For calculations see Excel sheet '9. Pharmaceutical experiments'

	Avg. removal efficiency [%]	**Minimum** [%]	**Maximum** [%]	**Experiments**
Circulation + UV	4.82	4.60	5.04	2
Nanobubbles	4.06	3.79	4.33	2
Nanobubbles + UV	6.35	6.02	6.67	2

5 Discussion

In this project the concentration is high for the substances used i.e. methylene blue, diclofenac and venlafaxine considering the application in this project. For the degradation of methylene blue as well as the APIs the degradation as a result of the combination of nanobubbles and UV light compared to UV only is modest, although the fraction out of the total degradation is larger for venlafaxine. The general concern is that concentrations of methylene blue and APIs respectively are too high relative to the concentration of nanobubbles. The main challenge in this regard has been that it was not possible to measure the concentration of nanobubbles. This will be discussed further in Section 5.2 and Section 5.3.

Looking into an novel topic such as nanobubbles and oxidation of APIs, another challenge has been the availability of published material. Hence a lot of effort has been put into the settings of equipment, piecing together information from related field of research and making assumptions based on this.

5.1 Nanobubbles

As mentioned in Section 2.5 it has been difficult to determine the properties of the nanobubbles produced as it has been challenging to measure especially the size distribution and zeta potential of the nanobubbles. Therefore it is problematic to conclude whether or not nanobubbles were generated. There is of course many indications that the experimental setup has been able to produce nanobubbles e.g. the size distributions although the mean peak is not as low as stated by Moleaer, see Chapter 2.

There are different factors that could affect the results for the nanobubbles. The unit producing the nanobubbles could be faulty and it is very difficult to establish for certain. In addition the instrument used to determine measurements is not what Moleaer suggests i.e. a NTA. The main feature that the Zetasizer Nano ZS used in this project lacks compared to the NTA measurements of the concentration of nanobubbles. Instead the concentration had to estimated based on literature. Measuring the concentration would have been another method for providing evidence of the production of nanobubbles. Furthermore, one of the challenges in terms of the DLS method is that results may be affected by impurities in the samples. This has been difficult to avoid entirely considering the open system of the experimental setup, see Figure 2.2 and Figure 2.3. This was particularly the case when using a compressor for the supply of atmospheric air. This may explain the second peak at approximately 8,000 nm in Figure 2.8 to Figure 2.10. This could indicate that there are some larger particles in the samples.

The setting used for the DLS measurements are backscatter normal resolution. Here it could be argued that high resolution may be better than normal resolution as the mean particle size detected is slightly lower, see Table 2.5. However, this is based on two samples and would need further verification.

In Table 2.6 it can be seen that there are measurements with good data quality. It also shows the difference in average size distribution with all 10 measurements as well as the average size distributions where only measurements of good data quality are included. E.g. on 06.02.23 the average size distribution of the nanobubbles after 45 mins is 395 ± 46 nm for all 10 measurements. For the 7 measurements with good data quality the average size distribution is 366 ± 45 nm. This is an indication that even though data quality is not good, it may not affect the results.

The oxygen level was measured using a modified Winkler method, where acid was added in order to provoke a collapse of the nanobubbles. The thesis was that by bursting the nanobubbles, the oxygen contained in the nanobubbles would be dissolved in the solution. Table 2.2 shows the results from the Winkler experiments which indicates that additional oxygen is dissolved. These values are only based on one experiment but it may give an indication of how much oxygen is contained in the nanobubbles. As the release of oxygen was not instantaneous, the acidity may need to be increased to speed up the collapse of the nanobubbles.

The zeta potential measurements are as stated in Section 2.5.3 within an interval of -13 mV to -20 mV. This is somewhat in agreement with what Moleaer says which is approximately -25 mV in clean water Moleaer [n/aa]. The literature in general gives a larger interval of zeta potential in nanobubbles from -15 mV to -45 mV. The larger interval is in better correspondence with the results found in this project even though it is in the lower range of the interval. Meegoda et al. [2018] found that in a solution with a pH-value of 7 at 20 °C, oxygen nanobubbles had a zeta potential of -20 ± 5 mV and a size of 179 ± 82 nm. This is somewhat in agreement with what was found on 21.03.23 where the average temperature was 19.6 °C and the pH was 7.3. Here the size distribution after 45 min is 291 ± 36 nm and the zeta potential is -20 ± 1 mV. See table 2.7. It has not been possible to find other references to support these findings. Since the zeta potential value is dependant on the size of the nanobubbles, the difference in zeta potential could be explained by the higher mean peak in the size distributions of this report relative to the results found by Meegoda et al. [2018]. Another explanation for the difference in results could be because the hydrodynamic cavitation method with micro- and nano-sized nozzles was to used by Meegoda et al. [2018] to generate nanobubbles rather than shear.

The zeta potential was investigated at different pH values in order to see how sensitive the value is to changes in pH. In the article made by Meegoda et al. [2018] the zeta potential was also measured at different pH-values ranging from 4 to 10 with oxygen nanobubbles at 20 °C. It was found that as the pH increases the zeta potential shifts from positve to increasingly negative values. Meegoda et al. [2018] found that at a pH-value of 4 the zeta potential was measured to be -4.3 mV and at a pH-value of 10 it became -27.3 mV. This matches the results found in the experiments, even though the values for the zeta potential in this project is lower at pH 9.5 and higher at pH 4, see Figure 2.11. This along with results from the modified Winkler method suggest that the addition of acid to samples

could be used as a tool for bursting the nanobubbles and for documenting nanobubbles in water samples.

In this report the method for generating nanobubbles was shear from a membrane surface, but other methods could be explored e.g. sonication as this method could both generate and burst nanobubbles. However, UV light and shear nanobubble generators are already commercially produced for full scale wastewater treatment plants, whereas sonication is at the lowest possible technology readiness level.

5.2 Oxidative capacity of nanobubbles

The methylene blue concentration of 0.16 mM for the experiments was chosen based on articles where the Fenton reaction was used to degrade methylene blue as no literature could be found on nanobubbles and the degradation of methylene blue. Methylene blue was efficiently degraded to an absorbance of 0 within seconds using the Fenton reaction as described in Section 3.2.2. For the initial experiments with methylene blue in 200 mL samples using experimental setup 1, see Figure 3.2, there was no consistent results indicating that methylene blue was degraded. As a result the sample volume was decreased to 43 mL and the experimental setup was changed to setup 2, see Figure 3.3 to ensure constant exposure of the sample to the UV light. Final experiments were conducted using experimental setup 1 and reducing the volume to 150 mL which was the least possible using this setup. Results shared by Molear in May indicate that degradation of methylene blue could have been achieved at a methylene blue concentration of $0.3 \cdot 10^{-3}$ mM.

Ideally a stock solution had been made, but this was not possible for the nanobubble samples as they were capped and kept closed until the start of each experiment. As mentioned earlier the stability of nanobubbles has not been clearly documented as different references mentions a "lifespan" ranging from hours to months. An alternative could have been to make a stock solution in BOD water that was concentrated enough to achieve the final concentration when mixed into the nanobubble sample. However that would reduce the concentration of nanobubbles in the final sample for the experiment, which is not ideal considering that the sample volume is only 150 mL. In addition methylene blue is difficult to dissolve evenly and has to be constantly stirred to ensure complete mixing in the sample. For this reason, focus was kept on accurate measuring of methylene blue and solute for each experiment.

In addition to adjusting the concentration of methylene blue other aspects of exogenous forces to generate a collapse of nanobubbles could be assessed. UV light as an exogenous force could be explored further as the only wavelength explored was 254 nm, but other wavelenghts may potentially yield better results. As mentioned in Section 3.1 exposing nanobubbles to sonication could be another way of generating hydroxyl radicals. Yasuda et al. [2019] argued that a significant reduction in nanobubble concentration was only observed at frequencies 488 kHz and 1 MHz, but this conclusion may be biased by differences in sonication equipment i.e. at 22, 43 and 129 kHz compared to at frequencies 488 kHz and 1 MHz. Little published material is available on this topic and it would have to be explored further. In addition, the use of sonication would require a more complex experimental setup incl. signal generation, a power amplifier and a transducer etc.

5.3 Degradation of active pharmaceutical ingredients

One major challenge in relation to the detection of APIs in the water environment is that attempts to map the extent of the problem has been limited by the costs of the conventional target analysis i.e. detection of one selected substance. Implicitly, only the APIs tested for, will be found. Hence this report builds on APIs where the concentrations above PNEC have been documented. Presumably there will be a considerable number of APIs and other chemicals of emerging concern that are not detected because analysis was not included in the measurement campaigns due to cost. Many additional substances are likely to be found as a result of broader screenings using non-target analysis such as QTOF.

Concentrations higher than the PNEC values have been tested in this study due to the use of HPLC analysis. The concentrations of diclofenac and venlafaxine in the experiments were set in order to exceed the HPLC limit of quantification to be able to measure the degradation. Refering back to the initial discussion of concentrations, the concentration of APIs in relation to the nanobubble concentration might have been to high to detect a degradation. Ideally concentrations of diclofenac and venlafaxine at 0.01 g L^{-1} or below had been tested to see if a higher degradation efficiency could be detected, as this would potentially increase the nanobubble concentration relative to the API concentration. As mentioned in Section 4.4.1 the majority of the degradation of diclofenac is caused by UV light, see Figure 4.3 to Figure 4.6. The degradation of diclofenac can be seen in Table 4.4. A small difference is observed in removal efficiency when comparing results from nanobubbles combined with UV light (84.7%) to UV light only (81.8%). Hence, you could argue that even though the removal efficiency is increased when combining UV light and nanobubbles compared to UV ligth only, the addition to the removal efficiency is small in relation to wastewater treatment processes. In particular considering the requirements proposed in the revision of the European urban wastewater treatment directive.

To separate the effects of circulation, nanobubbles and UV light, four categories of experiments were conducted for degradation of methylene blue as well as APIs, see Section 3.3. However, the effects of circulation was not tested in the experiments on venlafaxine. This was based on the results from diclofenac experiments, as the degradation of diclofenac from circulation alone was insignificant relative to the effects from UV. Subsequently the results showed that the degradation of venlafaxine was much lower than for diclofenac. Thus, for venlafaxine, the fraction of the degradation resulting from circulation is supposedly relatively larger than for diclofenac. Ideally experiments testing venlafaxine and circulation only should have been conducted to determine the effect of circulation.

A final remark on the experimental setup concerns the volume of 220 L that is circulated. This prevents testing of API degradation as the water passes the pump and membrane. This would result in pressure changes that may act as an exogenous force resulting in a collapse of the nanobubbles. In this scenario, degradation as a result of circulation may be considerably higher than results in this report indicate.

6 Conclusion

In this report the degradation of two APIs commonly found in the effluent of Danish wastewater treatment plants was tested. Diclofenac and venlafaxine at concentrations of 0.1 g L^{-1} dissolved in 150 mL nanobubble samples was appraised during exposure to UV_{254} light.

The degradation of diclofenac was primarily caused by UV light. The mean degradation of diclofenac in a nanobubble sample exposed to UV light for an hour is 84.7% with a range of 83.9% to 85.5% and a coefficient of determination between 0.997 and 0.998. This is slightly more than the average degradation of diclofenac in a sample that does not contain nanobubbles and is exposed to UV only. For this scenario the average degradation is 81.8% with a range of 81.3% to 82.3% and a coefficient of determination of 0.999. For the both scenarios it is a second order degradation rate. The degradation from circulation in the experimental setup as well as degradation from circulation in the experimental setup combined with nanobubbles was tested, but correlation was to poor to make conclusions on this result.

Venlafaxine showed a zero order degradation rate and as expected was found to be less sensitive to UV degradation. The mean degradation of venlafaxine in a nanobubble sample exposed to UV light for an hour is 6.35% with a range of 6.02% to 6.67% and a coefficient of determination between 0.987 and 0.998. This is slightly more than the average degradation of venlafaxine in a sample that does not contain nanobubbles and is exposed to UV only. For this scenario the average degradation is 4.82% with a range of 4.60% to 5.04% but the coefficient of determination for these experiments was however considerably lower for these experiments ranging from 0.607 to 0.833. The average degradation from circulation in the experimental setup combined with nanobubbles was 4.06% ranging from 3.79% to 4.33%. The coefficient of determination was 0.954 and 0.971 respectively for the two experiments.

For both APIs the average degradation for one hour is slightly higher for the combination of nanobubbles and UV, than for nanobubbles or UV light alone, although the fraction out of the total degradation is larger for venlafaxine. If hydroxyl radicals are formed the concentration is not sufficient to significantly degrade spiked samples of sodium diclofenac or venlafaxine hydrochloride.

Two methods were appraised for the documentation of nanobubbles; a Zetasizer nano ZS and a modified Winkler titration method to measure the oxygen content in samples. The Zetasizer nano ZS using DLS can be applied to assess the content of nanobubbles in clean water samples. The ion strength has to be increased as the zetasizer cannot analyse samples properly in demineralised water. This can solved by adding solutions normally

used for BOD testing. Backscatter and normal resolution was found to be the optimum setting for the zetasizer based on runtime for the analysis and the number of results with good data quality. The mean diameter of the nanobbles measured was in the range 256 to 484 nm. High resolution may yield the same data quality and a smaller mean size relative to normal resolution for the same sample, but this would require further tests to confirm. The modified Winkler titration method was tested as a second method as this could potentially be used for analysis of water samples from a less controlled setting than a laboratory. The modification consisted in adding acid to destabilise the nanobubbles in the sample. The dissolved oxygen content at the beginning of the experiment was 8.45 mg L^{-1} and the saturation level 8.73 mg L^{-1}. No increase in dissolved oxygen was measured after three hours, but after 48 hours the dissolved oxygen had increased from 8.45 mg L^{-1} to 10.0 and after 7 days the dissolved oxygen was measured to be 11.6 mg L^{-1}. This could be a method for documenting nanobubbles in collected environmental water samples.

Benzoic acid and methylene blue was considered as indicators of hydroxyl radicals formed by the collapse of nanobubbles. Benzoic acid is not suited for the purpose as the formation of the iron complex as a result of the degradation of benzoic acid requires acidic conditions which is not compatible with nanobubbles. For a concentration of 0.16 mM methylene blue no consistent results were achieved during the testing of methylene blue degradation.

7 Suggestions for further research

Although the combination of nanobubbles and UV - compared to UV alone - did not result significantly contribute to the degradation of methylene blue or the selected APIs, further research is relevant in terms of testing lower concentrations of APIs. In this project only spiked samples were analysed, when the PNEC values of the substances are even lower than what can be detected using HPLC.

It would be interesting to measure the impact on API concentrations at a full scale wastewater treatment plant using a QTOF screening before and after implementation of a nanobubble generator. Potentially combined with target analysis of selected APIs including diclofenac and venlafaxine. Ideally this is combined with a sidestream UV unit or the effects of natural UV radiation is observed.

In this project UV light at 254 nm was tested as an exogenous force to burst nanobubbles, but the use of UV light could be explored further by investigating other wavelengths. Furthermore the use sonication could also as an exogeneous force to burst nanobubbles as well as a method of generating nanobubbles.

Finally the optic oxygen sensor method could be explored further to document and potentially quantify the nanobubbles by logging the release of oxygen beyond three hours observed in this project. Also the modified Winkler method could be investigated further as the DLS and NTA methods are only applicable in clean water, so developing a method of analysis that could be used for less clean samples would be a useful tool if the nanobubble technology is to be implemented at wastewater treatment plants.

Bibliography

Abril et al., 2000, modified in 2007. G. Abril, M. Hesselsøe and A. H. Nielsen. *Oxygen measurement by Winkler Titration*, Aalborg University, 2000, modified in 2007.

Agarwal et al., 2011. Ashutosh Agarwal, Wun Jern Ng and Yu Liu. *Principle and application of microbubble and nanobubble technology for water treatment.* Chemosphere, 84, p. 1175–1180, 2011.

AlHesibri et al., 2016. Muidh AlHesibri, Jing Qian, MArie Jehannin and Vincent S. J. Craig. *A History of Nanobubbles.* Langmuir, 32, p. 11086 – 11100, 2016.

Atkinson et al., 2019. Ariel J. Atkinson, Onur G. Apul, Orren Schneider, Sergi Garcia-Segura and Paul Westerhoff. *Nanobubble technologies offer opportunities to improve water treatment.* Accounts of chemicals research, 52/2019, p. 1106–1205, 2019.

Azevedo et al., 2016. A. Azevedo, R. Etchepare, S. Calgaroto and J. Rubio. *Aqueous dispersions of nanobubbles: Generation, properties and features.* Minerals Engineering, 94, p. 29 – 37, 2016.

Bailon et al., 2021. Laura Bailon, Karen Klarskov Møller, Thomas Møller, Mette Schrøder Hansen and Boris Schuleit. *Kortlægning af lægemiddelstoffer i spildevand samt fjernelse af disse - redegørelse på basis af analyseprogram på Aarhus Universitetshospital samt Egå renseanlæg*, Aarhus Vand and Aarhus Universitetshospital and Aarhus kommune, 2021.

Bayley, 2022. Carina Cupit Bayley. *Screening for medicinrester og miljøfremmede stoffer v. Skanderborg Forsyning.* URL https://www.atv-jord-grundvand.dk/wp-content/uploads/2022/06/Moede-89-Carina-Cupit-Bayley-Screening-for-medicinrester.pdf. Cited: May 2023.

Behroozi, 2022. Fred Behroozi. *A Fresh Look at the Young-Laplace Equation and its Many Applications in Hydrostatics.* The Physics teacher, 60, p. 358 – 361, 2022.

Bu and Alheshibri, 2021. Xiangning Bu and Muidh Alheshibri. *The effect of ultrasound on bulk and surface nanobubbles: A review of the current status.* Ultrasonics Sonochemistry, 76, p. 105629, 2021.

ChemSrc, n/a. ChemSrc. *Benzoic acid.* URL https://www.chemsrc.com/en/cas/65-85-0_951954.html. Cited: June 2023.

Cole-Parmer, **n/a**. Cole-Parmer. *Environmental express BOD dilution water reagent set, P/Mg/Ca/Fe, 500 mL of each*. URL https://www.coleparmer.com/i/environmental-express-bod-dilution-water-reagent-set-p-mg-ca-fe-500-ml-of-each/5320032. Cited: December 2023.

Collins and Bolton, **2016**. James Collins and Jim Bolton. *Advanced oxidation handbook*. ISBN:978-1-58321-984-3, 1st edition. American Waterworks Association, 2016.

Cuklev et al., **2011**. Filip Cuklev, Erik Kristiansson, Jerker Fick, Noomi Asker, Lars Förlin and D. G. Joakim Larsson. *Diclofenac in fish: Blood plasma levels similar to human therapeutic levels affect global hepatic gene expression*. Journal of Toxicology and Chemistry, 30, p. 2126 – 2134, 2011.

da Silva et al., **1998**. Joaquim C.G. Esteves da Silva, Adélio A.S.C. Machado and César J.S. Oliveira Laquipai. *Effect of pH on complxication of Fe(III) with fulvic acids*. Environmental Toxicology and Chemistry, 17, p. 1268 – 1273, 1998.

DANVA, **2021**. DANVA. *Medicinrester i spildevand og vandmiljø*, 2021.

DANVA, **n/a**. DANVA. *Demonstration af metoder til reduktion af bromat produceret ved ozonering af spildevand med henblik på reduktion af miljøfremmede stoffer*. URL https://www.danva.dk/viden/vudp/projektuddelinger/demonstration-af-metoder-til-reduktion-af-bromat-produceret-ved-ozonering-af-spildevand. Cited: May 2023.

DCE and GEUS, **2017**. DCE and GEUS. *Det nationale overvågningsprogram for vandmiljø og natur 2017-21 Programbeskrivelse*, Miljøstyrelsen, 2017.

DHI, **2013**. DHI. *Forslag til administrationsgrundlag for lægemiddelstoffer i hospitalsspildevand - Anbefalede maksimale koncentrationer ved tilslutning til kloak Input til KL's Arbejdsgruppe omkring hospitalsspildevand*, 2013.

DHI and EKJ, **2021**. DHI and EKJ. *Spildevandsteknisk beskrivelse for nyt OUH*, Region Syddanmark, 2021.

Directorate General for Environment, **n/a**. Directorate General for Environment. *Proposal for a revised Urban Wastewater Treatment Directive*. URL https://environment.ec.europa.eu/publications/proposal-revised-urban-wastewater-treatment-directive_en. Cited: December 2022.

Drastrup, **2022**. Ellen Marie Drastrup. *Renseteknologier til fjernelse af medicinrester*. URL https://www.atv-jord-grundvand.dk/wp-content/uploads/2022/06/Moede-89-Ellen-Drastrup-Renseteknologier.pdf. Cited: May 2023.

Dutta et al., **2001**. Kabita Dutta, Subrata Mukhopadhyaya, Sekhar Bhattacharjee and Basab Chaudhuri. *Chemical oxidation of methylene blue using a Fenton-like reaction*. Journal of Hazardous Materials, B84, p. 57 – 71, 2001.

Elma Instruments, **n/a**. Elma Instruments. *Manual ELMA 795*, Elma instruments, n/a.

Eurofins, **n/a**. Eurofins. *Webinar om QTOF og non-target screeninger*. URL https://www.eurofins.dk/miljoe/nyheder/qtof-webinar/. Cited: April 2023.

Ewelina Dziurkowska, **2013**. Marek Wesolowski Ewelina Dziurkowska. *Simultaneous quantitation of venlafaxine and its main metabolite, O-desmethylvenlafaxine, in human saliva by HPLC*. Journal of separation science, 33, p. 1726 – 1733, 2013.

Harris and Lucy, **2019**. Daniel C. Harris and Charles A. Lucy. *Quantitative chemical analysis*. ISBN: 9781319324506, 10th edition. W.H. Freeman and Company, 2019.

Hashimoto et al., **2022**. Kurumi Hashimoto, Atsushi Onzuka, Wataru Nishijima, Masashi Yamazaki, Michiko Aoki and Tomomi Sao. *Effect of fine bubbles for washing of monolith type porous ceramic membranes treating oil-in-water emulsions*. Chemophere, 305, p. 1 – 8, 2022.

Ikonen et al., **2021**. Jenni Ikonen, Ilpo Nuutinen, Marjo Niittynen, Anna-Maria Hokajärvi, Tarja Pitkänen, Eero Antikainen and Ilkka T. Miettinen. *Presence and Reduction of Anthropogenic Substances with UV Light and Oxidizing Disinfectants in Wastewater — A Case Study at Kuopio, Finland*. Water, 13, p. 360, 2021.

Jadhav et al., **2021**. Ananda J. Jadhav, Gianluca Ferraro and Mastafa Barrigou. *Generation of Bulk Nanobubbles Using a High-Shear Rotot-Stator Device*. Industrial and Engineering Chemistry Research, 60, p. 8597–8606, 2021.

Jensen et al., **2022**. Nana Wirenfeldt Jensen, Tahereh Faraji, Adriana Gonzalez Ospina, Ronan Guillosso, Francoise Petitpain Perrin, Per Krøyer Kristensen, Susan Hove Hansen, Mads Koustrup, Morten Boel Overgaard Andersen, Christia Tranekær and Micheal Lind-Frendsen. *Removal of micropollutants by application of multiple point ozonation and powder activated carbon*, The Danish Environmental Protection Agency, 2022.

Jr et al., **2014**. Joseph H. Bisesi Jr, William Bridges and Stephen J. Klaine. *Effects of the antidepressant venlafaxine on fish brain serotonin and predation behavior*. Aquatic Toxicology, 148, p. 130 – 138, 2014.

Kikuchi et al., **2009**. Kenji Kikuchi, Aoi Ioka, Yoshinori Tanaka, Yasuhiro Saihara and Zempachi Ogumi. *Concentration determination of oxygen nanobubbles in electrolyzed water*. Journal of Colloid and Interface Science, 329/2009, p. 306–309, 2009.

Liu and Guoxin, **2016**. Hailong Liu and Guoxin. *Effectiveness of the Young-Laplace equation at nanoscale*. Scientific reports, 6, p. 1 – 10, 2016.

Liu et al., **2016**. Shu Liu, Seiichi Oshita, Saneyuki Kawabata, Yoshio Makino and Takahiko Yoshimoto. *Identification of ROS Produced by Nanobubbles and Their Positive and Negative Effects on Vegetable Seed Germination*. Langmuir, 32/2016, p. 11295–11302, 2016.

Loligo Systems, **n/a**. Loligo Systems. *Witrox-1/4 user manual - wireless fiber optic oxygen instrument for mini sensors*, Loligo Systems, n/a.

Loos et al., 2018. Marinov Loos, R., I. D., Sanseverino, D. Napierska and T. Lettieri. *Review of the 1st Watch List under the Water Framework Directive and recommendations for the 2nd Watch List*, Publications Office of the European Union, 2018.

Malvern, April 2013. Malvern. *Zetasizer nano series user manual*, Malvern, April 2013.

Maulvault et al., 2018. Ana Luísa Maulvault, Lúcia H.M.L.M. Santos, José Ricardo Paula, Carolina Camachoa, Vasco Pissarra, Fabiola Fogaça, Vera Barbosa, Ricardo Alvesa, Pedro Pousão Ferreira, Damià Barceló, Sara Rodriguez-Mozaz, António Marques, Mário Diniz and Rui Rosa. *Differential behavioural responses to venlafaxine exposureroute, warming and acidification in juvenile fish(Argyrosomusregius)*. Science of the Total Environment, 634, p. 1136 – 1147, 2018.

Meegoda et al., 2018. Jay N. Meegoda, Shaini Aluthgun Hewage and Janitha H. Batagoda. *Stability of Nanobubbles*. Environmental engineering Science, 35, p. 1216–1225, 2018.

Melgoza et al., 2009. D. Melgoza, A. Hernández-Ramírez and J. M. Peralta-Hernández. *Comparative efficiencies of the decolourisation of Methylene Blue using Fenton's and photo-Fenton's reactions*. Photochemical Photobiological Sciences, 8, p. 596 – 599, 2009.

Merck, n/aa. Merck. *Diclofenac Sodium*. URL https://www.sigmaaldrich.com/DK/en/substance/diclofenacsodium3181315307796. Cited: May 2023.

Merck, n/ab. Merck. *Methylene blue*. URL https://www.sigmaaldrich.com/DK/en/product/mm/159270. Cited: June 2023.

Merck, n/ac. Merck. *Venlafaxine hydrochloride*. URL https://www.sigmaaldrich.com/DK/en/substance/venlafaxinehydrochloride3138699300784. Cited: May 2023.

Michailidi et al., 2020. Elisavet D. Michailidi, George Bomis, Athanasios Varoutoglou, George Z. Kyzas, George Mitrikas, Athanasios Ch. Mitropoulos, Eleni K. Efthimiadou and Evangelos P. Favvas. *Bulk nanobubbles: Production and investigation of their formation/stability mechanism*. Journal of Colloid and Interface Science, 564/2020, p. 371–380, 2020.

Miljøministeriet, 2018. Miljøministeriet. *Vejledning til bekendtgørelse om spildevandstilladelser m.v. efter miljøbeskyttelseslovens kapitel 3 og 4*. URL https://www.retsinformation.dk/eli/retsinfo/2020/9568. Cited: May 2023.

Miljøstyrelsen, 1998. Miljøstyrelsen. *Miljøvurdering*. URL https://www2.mst.dk/udgiv/Publikationer/1998/87-7909-097-4/html/kap11.htm. Cited: May 2023.

Miljøstyrelsen, 2006. Miljøstyrelsen. *Tilslutning af industrispildevand til offentlige spildevandsanlæg - Vejledning fra Miljøstyrelsen Nr. 2 2006*. URL https://www2.mst.dk/Udgiv/publikationer/2006/87-7052-055-0/pdf/87-7052-055-0.pdf. Cited: May 2023.

Minamoto et al., 2021. Chihiro Minamoto, Nonoka Fujiwara, Yutaka Shigekawa, Kaori Tada, Jun Yano, Takashi Yokoyama, Yoshikazu Minamoto and Susumu Nakayama. *Effect of acidic conditions on decomposition of methylene blue in aqueous solution by air microbubbles.* Chemosphere, 263, p. 128141, 2021.

Moleaer, n/aa. Moleaer. *Moleaer webpage.* URL https://www.moleaer.com/nanobubbles. Cited: April 2023.

Moleaer, n/ab. Moleaer. *Moleaer products lotus.* URL https://www.moleaer.com/products/lotus. Cited: April 2023.

Moleaer, n/ac. Moleaer. *Nanoparticles - The Science Behind Nanobubbles: An Introduction with Malvern Panalytical and Moleaer.* URL https://events.malvernpanalytical.com/W221206EPI-NTA-nanobubble. Cited: December 2022.

Moleaer, n/a. Moleaer. *Teams meeting*, Unpublished, n/a.

Naturstyrelsen, 2015. Naturstyrelsen. *NOVANA Screeningsundersøgelse for humane lægemidler i vandmiljøet*, Miljøstyrelsen, 2015.

pro.medicin.dk, 2023. pro.medicin.dk. *Efastad - Venlafaxin.* URL https://pro.medicin.dk/Medicin/Praeparater/8969. Cited: June 2023.

Raut et al., 2003. B. B. Raut, B. L. Kolte, A. A. Deo, M. A. Bagool and D. B. Shinde. *A Rapid and Sensitive HPLC Method for the Determination of Venlafaxine and O-Desmethylvenlafaxine in Human Plasma with UV Detection.* Journal of Liquid Chromatography Related Technologies, 26, p. 1297 – 1313, 2003.

Satoh et al., 2007. Andrea Y. Satoh, James E. Trosko and Susan J. Masten. *Methylene blue dye test for rapid qualitative detection of hydroxyl radicals formed in a Fenton's reaction aqueous solution.* Environmental Science and Technology, 41, p. 2881 – 2887, 2007.

Soheili-Azad et al., 2020. Payam Soheili-Azad, Mohammad Reza Yaftian and Mir Saeed Seyyed Dorraji. *Zn/Al-layered double hydroxide–graphene oxide nanocomposite use in the solid-phase extraction–preconcentration and HPLC determination of diclofenac.* Chemical Papers, 74, p. 4419 – 4432, 2020.

Soyluoglu et al., 2021. Meryem Soyluoglu, Daekyun Kim, Yeakub Zaker and Tanju Karanfil. *Stability of Oxygen Nanobubbles under Freshwater Conditions.* Water Research, 206, p. 117749, 2021.

Stapf et al., n/a. Michael Stapf, Veronika Zhiteneva and Ulf Miehe. *WWTP fitness check - Results from Danish WWTPs.* URL https://projects.au.dk/fileadmin/www.waterpurification.au.dk/CWPharma_2/9_Stapf.pdf. Cited: April 2023.

Stuer-Lauridsen et al., n/a. Frank Stuer-Lauridsen, Lisbet Hansen, Morten Birkved, Jesper Kjølholt and Sonja Mikkelsen. *Litteraturudredning vedrørende human medicin i miljøet; Eksponering af og effekt på mennesker.* URL https://www2.mst.dk/udgiv/publikationer/2002/87-7944-998-0/html/kap08.htm#top. Cited: May 2023.

Takahashi et al., 2017. Masayoshi Takahashi, Kaneo Chiba and Pan Li. *Free-Radical Generation from Collapsing Microbubbles in the Absence of a Dynamic Stimulus.* The journal of physical chemistry, 11/2017, p. 1343–1347, 2017.

The Danish Environmental Protection Agency, n/a. The Danish Environmental Protection Agency. *Vandrensning ved hjælp af aktiv kulfiltre: 2 Kemiske stoffers tilbageholdelse i aktiv kul – Internationale erfaringer.* URL https://www2.mst.dk/udgiv/publikationer/1998/87-7909-126-1/html/kap02.htm#kap02. Cited: April 2023.

The Danish Environmental Protection Agency, 2022. The Danish Environmental Protection Agency. *MerEFF - Environmental treatment of wastewater effluents MiljøEffektiv Rensning af afløb fra renseanlægs EFFluenter*, The Danish Environmental protection agency, 2022.

The Danish Environmental Protection Agency, 2021. The Danish Environmental Protection Agency. *Kortlægning af renseteknologier - Til målrettet spildevandsrensning for metaller og miljøfremmede stoffer på centralrenseanlæg*, Miljøministeriet, 2021.

Ushikubo et al., 2010. Fernanda Yumi Ushikubo, Takuro Furukawa, Ryou Nakagawa, Masatoshi Enari, Yoshio Makino, Yoshinori Kawagoe, Takeo Shiina and Seiichi Ashita. *Evidence and the existence and the stability of nano-bubbles in water.* Colloids and Surfaces A: Physicochemical and engineering aspects, 361, p. 31–37, 2010.

Weast, 1977. Robert C. Weast. *Handbook of chemistry and physics.* ISBN:n.a., 58th edition. CRC Press, 1977.

Wu et al., 2019. Leichao Wu, Yong Han, Qianrui Zhang and Shuai Zhao. *Effect of external electric field on nanobubbles at the surface of hydrophobic particles during air flotation.* RSC Advances, 9, p. 1792–1798, 2019.

Xylem, 2015. Xylem. *Operating manual: Multi 3430 - digital meter for digital IDs sensors*, Xylem, 2015.

Yasuda et al., 2019. Keiji Yasuda, Hodaka Matsushima and Yoshiyuki Asakura. *Generation and reduction of bulk nanobubbles by ultrasonic irradiation.* Chemical Enigineering Science, 195, p. 455 – 461, 2019.

Yasui et al., 2018. Kyuichi Yasui, Toru Tuziuti and Wataru Kanematsu. *Mysteries of bulk nanobubbles (ultrafine bubbles); stability and radical formation.* Ultrasonics - Sonochemistry, 28, p. 259–66, 2018.

yu Zhang et al., 2020. Xu yu Zhang, Qian shuai Wang, Zhong xian Wu and Dong ping Tao. *An experimental study on size distribution and zeta potential of bulk cavitation nanobubbles.* Internatal Journal of Minerals, Metallurgy and Materials, 27, p. 152–161, 2020.

A Oxygen measurement using the Winkler titration method

The sections A.1 to A.5 describing the laboratory experiments using the Winkler titration is from the protocol of Winkler by Abril et al. [2000, modified in 2007] including a few elaborations for the purpose of this project. Furthermore the article by Kikuchi et al. [2009] which describes a modified Winkler method is clearly referenced when applied.

Based on Kikuchi et al. [2009] the modifications of the traditional Winkler method in this project are:

- The volume of the Winkler flask is filled with 1/5 water containing nanobubbles and 4/5 oxygen free water
- Sulfuric acid is added to the water sample in Winkler bottle, as the acid will burst the nanobubbles in the water, and thereby increase the dissolved oxygen concentration [Kikuchi et al., 2009]

A.1 Principle of Winkler method

The following reactions are describing what happens in the Winkler titration:

Reaction 1a: $MnCl_2 + 2NaOH \rightarrow Mn(OH)_2 + 2Na^+ + 2Cl^-$

Reaction 1b: $\frac{1}{2}O_2 + Mn(OH)_2 \rightarrow MnO(OH)_2$

Reaction 2: $MnO(OH)_2 + H_2SO_4 + 2NaI \rightarrow Mn(OH)_2 + NaSO_4 + H_2O + I_2$

Reaction 3: $I_2 + 2Na_2S_2O_3 \rightarrow Na_2S_4O_6 + NaI$

Reaction 1a describes how adding a strong base to a solution containing iodie (solution 1) as well as a solution with a divalent manganese (solution 2) a precipitation of manganese hydroxide will happen. According to reaction 1b will the dissolved oxygen in the sample oxidize to an equal quantity of $Mn(OH)_2$ into $MnO(OH)_2$. The manganese complex will be destabilised because of the added acid ($H2SO_4$) and there will be a formation of a quantity of Iodine (I_2) equivalent to the original DO content. This is described in reaction 2. Reaction 3 shows Iodine being titrated with a standard solution of thiosulfate with a concentration of approximately 0.004 M.

Please note that when determining the concentration of the thiosulfate solution, the three reagents (solution 1, solution 2 and acid) is added the opposite way (i.e. acid, solution 2

and lastly solution 1) so the manganese complex and Iodine (I_2) is not formed. By then adding a known quantity of KIO_3, I_2 is produced by the following reaction:

$KIO_3 + 5I^- + 6H^+ \rightarrow 3I_2 + 3H_2O + K^+$

A.2 Preparation of reagents

The following solutions must be prepared:

Solution 1

Solution 1 is made of NaI (3M), $NaOH$ (8M) and demineralised water.

Materials:
100 ml measuring cylinder
3x250 ml beakers
2 stirring sticks
Scale

Procedure:

1. Dissolve 30g of NaI into 50 ml of demineralised water in a beaker
2. Dissolve 16g of $NaOH$ into 50 ml of demineralised water in another beaker
3. As the solutions get hot, let them cool down, and mix both solutions into one beaker

Solution 2

Solution 2 is made of $MnCl_2 : 4H_2O$ and demineralised water.

Materials:
100 ml measurement cylinder
250 ml beaker
Scale in fume hood

Procedure:
Dissolve 60g of $MnCl_2 : 4H_2O$ into 100 ml demineralised water in a beaker. NB This must be done in a fume hood as the chemical fumes are toxic.

Concentrated sulfuric acid

This does not need to be prepared, but make sure to be careful and use both gloves and safety glasses.

Thiosulfate solution

Thiosulfate is made of $Na_2S_2O_3 : 5H_2O$ and deionized water.

Materials:
100 ml measurement cylinder 250 ml beaker
Scale in the fume hood
1000 ml volumetric flask

Procedure:

1. Dissolve 1 g of $Na_2S_2O_3 : 5H_2O$ into a few ml deionised water (the exact amount is not important) in a volumetric flask. NB This must be done in the fume hood as the chemical fumes are toxic
2. Add 10 ml of conservation (see section below)
3. Fill deionized water into the solution until a total volume of 1000 ml

Conservation for the thiosulfate solution

The conservation is made of Na_2CO_3 and deionised water.

Materials:
50 ml beaker
25 ml measuring cylinder
Scale

Dissolve 0.1 g of Na_2CO_3 into 10 ml of deionized water.

Pottasium iodate

The pottasium iodate solution is made of $K(IO_3)$ and deionized water.

Materials:
100 ml measuring cylinder
1000 ml volumetric flask
Scale

Procedure:
Dissolve 0.3567 g of $K(IO_3)$ in approximately 200 ml deionized water. The exact amount is not important because when the $K(IO_3)$ is dissovled fill the volumetric flask up with demineralised water, so the total volume is 1000 ml.

Starch indicator

The starch indicator is made of $(C_6H_10O_5)n$ and demineralised water.

Materials:
Hot plate
250 ml beaker
100 ml beaker
100 ml measuring cylinder

Make a thin paste with 1 g of starch and a small amount of demineralised water. Bring 100 ml of demineralised water to a boil, remove it from the heat and mix into the starch paste.

Modified Winkler

The modification of Winkler is to add sulfuric acid with a concentration of 0.02 M into the sample in the Winkler flask before starting the traditional Winkler method. After

adding the acid is, and thereby lowering the pH level, some base must be added in order to increase the pH as the traditional Winkler is done at a neutral pH level [Kikuchi et al., 2009]. This is done by adding 0.3 mL of $NaOH$ with a concentration of 8M.

A.3 Standardisation of thiosulfate solution

As the thiosulfate solution is not stable i.e. the concentration will decrease over time, the concentration of the solution may vary with time and has to be determined every time the Winkler experiment is made. The concentration should be approximately 0.004 M. The procedure for the standardisation of the thiosulfate solution can be found in The Winkler Protocol [Abril et al., 2000, modified in 2007].

A.4 Dissolved oxygen measurement

When the concentration of the thiosulfate solution is known the dissolved oxygen can now be found. The procedure of the measurement of dissolved oxygen by using a modification of Winkler is as follows:

1. The winkler flask (approximately 60 mL, see Section A.6) is to be filled with 1 part nanobubble water and 4 parts oxygen free water, i.e. 12 mL nanobubble water and 48 mL oxygen free water [Kikuchi et al., 2009].

2. Add 64 μL H_2SO_4 (18 M) to the Winkler flask [Kikuchi et al., 2009].

3. Leave the sample for the acid to burst the nanobubbles [Kikuchi et al., 2009].

4. Add 0.3 mL of the extra $NaOH$ (8M) and 0.30 mL of solution 1 and as well as 0.3 mL of solution 2 into the Winkler flask [Kikuchi et al., 2009].

From here the procedure is as for the standard Winkler titration method, see The Winkler Protocol [Abril et al., 2000, modified in 2007].

A.5 Calculations concentration of thiosulfate solution and dissolved oxygen

As described earlier, in order to find the dissolved oxygen in a sample, the molarity of the thiosulfate solution must be found.

Determination of the molarity of thiosulfatee

The molarity of thiosulfate solution is found by the following equation as given by Abril et al. [2000, modified in 2007]:

$$\frac{0.816}{X} = M$$

Where X is the amount of thiosulfate solution titrated in mL.

The 0.816 comes from adding 8 mL of $K(IO_3)$ in the thiosulfate solution, and making this reaction happen:

Reaction: $K(IO_3) + 5I^- + 6H^+ \rightarrow 3I_2 + 3H_2O + K^+$

The reactions shows that 3 moles of Iodine (I_2) is produced per mole of potassium iodate ($K(IO_3)$). This means that $8mL$ of $K(IO_3)$ with a concentration of $0.0017M$ produces:

$$8mL \cdot 3(\frac{mLI_2}{molS_2O_3{}^-2}) \cdot 0.0017\frac{molS_2O_3{}^-2}{L} = 0.0408mmolI_2$$

Remember $M = \frac{mol}{L}$

The next reaction is when thiosulfate and iodine reacts:

$I_2 + 2Na_2S_2O_3 \rightarrow Na_2S_4O_6 + 2NaI$

From this the concentration of the thiosulfate can be found from the following:

$$\frac{2\frac{molS_2O_3{}^-2}{molI_2} \cdot 0.0408mmolI_2}{XmL} = \frac{0.0816}{X}\frac{molS_2O_3{}^-2}{L} = \frac{0.0816}{X}M$$

Determination of dissolved oxygen

The oxygen concentration can be determined from the following:

$$O_2 = \frac{\frac{1molO_2}{4molS_2O_3{}^-2} \cdot A\frac{molS_2O_3{}^-2}{L} \cdot BmL}{60mL}$$

Where A is the thiosulfate solution concentration in M, B is the amount of thiosulfate titrated in mL (after the standardisation) and 60 mL is the volume of the Winkler flask used, i.e. the amount of sample analysed. Remember to change this, if another volume is used.

$\frac{1}{4}$ is the ratio between oxygen and thiosulfatee, i.e. for each oxygen molecule there is four thiosulfate molecules.

In order to get the oxygen concentration in mg/L the molar weight of O_2 must be multiplied. The molar weight of oxygen is 32 g/mol.

A.6 Results of the modified Winkler

The Winkler flask are weighed as it is only approximately 50 mL in each flasks and it is important to know the exact amount a Winkler flask contains. The Winkler flasks have been weighed first without water (flask and cork separately), then with water and weighed again in order to find the total volume.

Table A.1. Winkler flasks

Winkler flasks	**Without water** [g]	**With water** [g]	**Total volume** [mL]
Cork 1	17.02		
Flask 1	51.77		
Total 1	68.79	129.02	60.23
Cork 2	16.85		
Flask 2	51.57		
Total 2	68.42	128.85	60.43
Cork 3	17.06		
Flask 3	51.70		
Total 3	68.76	129.22	60.46
Cork 4	17.09		
Flask 4	53.22		
Total 4	70.31	130.15	59.84
Cork 5	16.98		
Flask 5	53.07		
Total 5	70.05	129.74	69.69
Cork 6	12.43		
Flask 6	53.31		
Total 6	65.74	125.51	59.77
Average			60.07

Table A.1 shows the weight and volume of the six Winkler flask. The average of the total volumes of the six Winkler flasks are 60.07 mL and there is therefore used a volume of 60 mL for all Winkler experiments.

Dissolved oxygen concentration in demineralised water

The following samples are all made in demineralised water and are made on different days, 30.11.2022, 07.12.2022, 13.12.2022 and 06.02.2023. The samples are taken from the nanobubble tank after it has run 30 mins, i.e. 10 times over the membrane except measurements made on 06.02.23 - here the nanobubble generator has run for 45 mins, making it 15 times over the membrane.

Measurement 30.11.2022

As described above the thiosulfate solution must be standardised before use, because it is not stable and will change molarity over time, but will roughly be around $0.004M$, see Section A.3. Table A.2 shows the amount of $Na_2S_2O_3 : 5H_2O$ added in mL as well as the molarity of the thiosulfate solution. The average molarity of all six experiment is $0.00376M$. The dissolved oxygen content is calculated based on different molarities which can be seen in table A.2.

Table A.2. Standardisation of thiosulfate solution 30.11.2022

Sample no.	$Na_2S_2O_3 : 5H_2O$ [mL]	**Molarity** [M]
1	22.04	0.00370
2	18.86	0.00433
3	25.60	0.00319
4	23.43	0.00348
5	20.09	0.00406
6	20.25	0.00403
Average 1-6		0.00376
Average 5+6		0.00405

After the molarity have been determined, the dissolved oxygen can be determined. This is done as described in section A.4.

The oxygen free water concentration on 30.11.2022 was approximately 3.5 %, i.e. $0.32mg/L$ and the experiment was done roughly 1.5 hours after the acid was added. Table A.3 shows the dissolved oxygen concentration with different molarities (which is shown in the table above A.2). The dissolved oxygen concentration varies from $1.389mg/L$ to $1.885mg/L$.

Table A.3. Dissolved oxygen measurement - 30.11.2022

Sample no.	$Na_2S_2O_3 : 5H_2O$ [mL]	O_2 Average M [mg/L]	O_2 Highest M [mg/L]	O_2 Lowest M [mg/L]	O_2 Average M (5+6) [mg/L]
1	2.90	1.453	1.673	1.233	1.564
2	2.94	1.473	1.696	1.250	1.586
3	3.34	1.674	1.927	1.420	1.802
4	3.32	1.664	1.915	1.411	1.791
5	3.95	1.979	2.279	1.679	2.131
6	3.16	1.584	1.823	1.343	1.705
Average	3.27	1.638	1.885	1.389	1.763

Measurement 05.12.2022

The next samples was taken on 05.12.2022. But the samples was made on 07.12.2022 and 13.12.2022, therefore standardisation on 2 different days. This was because we did not know how long it would take for the acid to burst the nanobubbles - therefore did we make 3 Winkler samples approximately 2 days (1 day og 20 hours) after the acid was added and 7 days after the acid was added.

The oxygen free water added to the samples on 05.12.2022 was $0.18mg/L$ and a water temperature of $20.6°C$. The dissolved oxygen concentration BEFORE the nanobubble generator was $8.28mg/L$ and the water temperature was $22.1°C$.

The dissolved oxygen concentration AFTER the nanobubble generator has run for 30 mins was $8.45mg/L$ and the water temperature was $22.1°C$.

Table A.4 and table A.5 shows the standardisation of thiosulfate solution at 07.12.2022 and 13.12.2022 respectively.

Table A.4. Standardisation of thiosulfate solution 07.12.2022

Sample no.	$Na_2S_2O_3 : 5H_2O$ [mL]	**Molarity** [M]
1	19.924	0.00410
2	19.507	0.00418
3	19.648	0.00415
Average	19.693	0.00414

Table A.5. Standardisation of thiosulfate solution 13.12.2022

Sample no.	$Na_2S_2O_3 : 5H_2O$ [mL]	**Molarity** [M]
4	20.297	0.00402
5	20.020	0.00408
6	20.171	0.00405
Average	20.163	0.00405

Table A.6 and table A.7 shows the dissolved oxygen concentration at 07.12.2022 and 13.12.2022, respectively. On 07.12.2022 it was approximately 2 days after the acid was added to the Winkler flask, and 13.12.2022 was approximately 7 days after the acid was added.

Table A.6. Dissolved oxygen measurement - 07.12.2022. The dissolved oxygen concentration is calculated based on the average M.

Sample no.	$Na_2S_2O_3 : 5H_2O$ [mL]	O_2 [mg/L]
1	3.569	1.972
2	3.676	2.031
3	1.701	0.940
Average	2.982	1.647

Table A.7. Dissolved oxygen measurement - 13.12.2022. The dissolved oxygen concentration is calculated based on the average M.

Sample no.	$Na_2S_2O_3 : 5H_2O$ [mL]	O_2 [mg/L]
4	3.417	1.844
5	4.867	2.626
6	4.664	2.517
Average	4.316	2.329

Measurement 06.02.2023

The next samples was taken on 06.02.2023. The oxygen free water added to the samples was $0.24 mg/L$ and a water temperature of $20.7°C$. The dissolved oxygen concentration BEFORE the nanobubble generator was $7.45 mg/L$ and the water temperature was $25°C$.

The dissolved oxygen concentration AFTER the nanobubble generator has run for 45 mins was $8.46 mg/L$ and the water temperature was $24.8°C$.

Table A.8 shows the standardisation of thiosulfate solution made on 06.02.23.

Table A.8. Standardisation of thiosulfate solution 06.02.2023

Sample no.	$Na_2S_2O_3 : 5H_2O$ [mL]	**Molarity** [M]
1	26.92	0.00303
2	22.05	0.00370
3	22.04	0.00370
4	20.65	0.00395
5	21.01	0.00388
Average	22.53	0.00365

Table A.9 show the dissolved oxygen concentration on 06.02.23.

Table A.9. Dissolved oxygen measurement - 06.02.2023. The dissolved oxygen concentration is calculated based on the average M. There was an air bubble in the Winkler flask in the first measurement.

Sample no.	$Na_2S_2O_3 : 5H_2O$ [mL]	O_2 [mg/L]
1	2.26	1.101
2	2.24	1.091
3	2.11	1.028
4	1.93	0.938
5	2.04	0.992
Average	2.114	1.030

B Optic oxygen sensor experiment

When determining the oxygen content with the modified Winkler method you get one oxygen content at one specific time. Therefore the optic oxygen sensor measurements have been made, measuring the oxygen content over time. This was to see if there was a correlation between the oxygen content in the Winkler experiment and the optic oxygen sensor experiment and thereby confirming the results from both experiments. In order to compare the two experiments the optic oxygen sensor flask was filled with 4/5 oxygen free water and 1/5 demineralised water containing nanobubbles as for the modified Winkler method.
The optic oxygen used in the project is the wireless fiber optic oxygen sensor from Loligo Systems [Loligo Systems, n/a]. Figure B.1 shows the set up of the optic oxygen sensor.

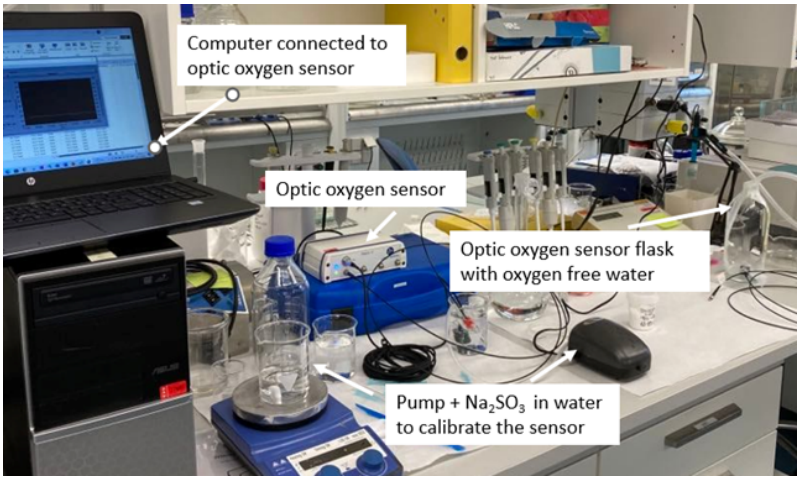

Figure B.1. The experimental setup of the optic oxygen sensor. It shows the optic oxygen sensor, the computer that is connected to the sensor, the optic sensor flask and what to use when calibrating the optic oxygen sensor.

Every time the optic oxygen sensor have to be used it needs to be calibrated with a high and a low oxygen content. The calibration data has been shown in the Table B.1, Table B.2 and Table B.3. In order to get the high oxygen content the sensor is put into a beaker with demineralised water and a small pump that aerate the water. When the oxygen content is approximately at saturation level, the high oxygen content is locked. In order to get the low oxygen content, the sensor is placed in a beaker with 100 mL demineralised water and 2 g of Na_2SO_3. This will use the oxygen in the water and thereby decrease the oxygen content. When the oxygen level is close to 0, i.e. 0.2 mg/L or below, the sensor is locked.

B.1 Optic oxygen sensor measurement in demineralised water on 30.11.2022

Calibration data 30.11.2022

Table B.1. Calibration data to the optic oxygen sensor, 30.11.2022. N is the N moving average. LO = low and HI = high. sat = saturation.

N	LO phase [r.U.]	HI phase [r.U.]	LO oxygen [% air sat.]	HI oxygen [% air sat.]	LO temp. [$°C$]	HI temp. [$°C$]
5	57.97	27.87	0	100	19.27	19.95

Figure B.2 shows the measurement made on 30.11.2022. This shows the time at the x-axis and the air saturation in [%] at the y-axis. At approximately 2000 sec there is a sudden drop in oxygen content and shortly afterwards it goes up again. This was because the sensor fell out of the sample and was out of the water for a few seconds. The optic oxygen sensor was in the sample for just over an hour, and was then stopped because the oxygen level did not change must and was at a constant level.

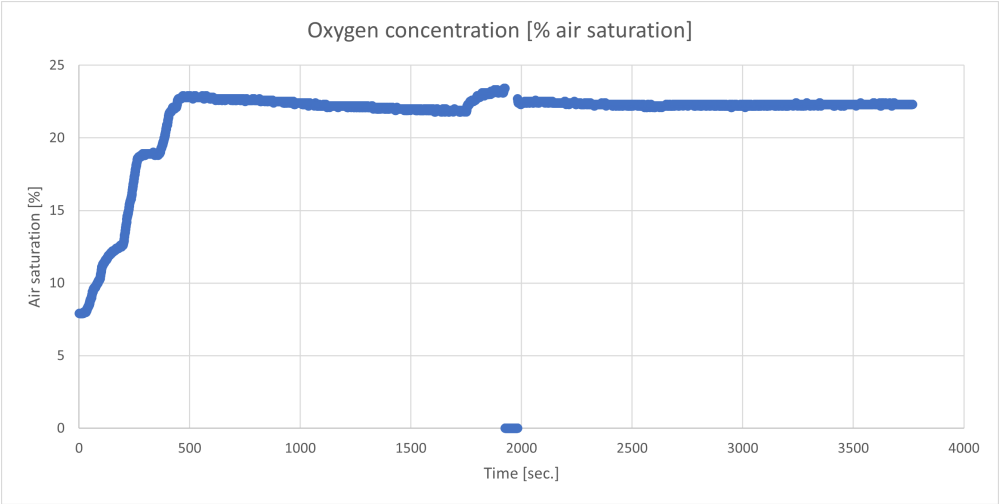

Figure B.2. Optic oxygen sensor measurement in 4/5 oxygen free demineralised water and 1/5 nanobubble water. The experiment was run on 30.11.2022

B.2 Optic oxygen sensor measurement in demineralised water on 13.12.2022

Calibration data 13.12.2022

Table B.2. Calibration data to the optic oxygen sensor, 13.12.2022. N is the N moving average. LO = low and HI = high. sat = saturation.

N	LO phase [r.U.]	HI phase [r.U.]	LO oxygen [% air sat.]	HI oxygen [% air sat.]	LO temp. [$°C$]	HI temp. [$°C$]
5	58.66	28.24	0	100	19.24	20.36

This experiments was made with some different parameters. There is still 4/5 oxygen free water and 1/5 nanobubble water in the optic oxygen sensor flask. It was thought that maybe the nanobubble water was put into the flask to slowly and there was tested another method. As it shows in Figure B.3 this method was not better as there is a peak at the beginning of the experiment. The run time for the experiment was increased to approximately three hours.

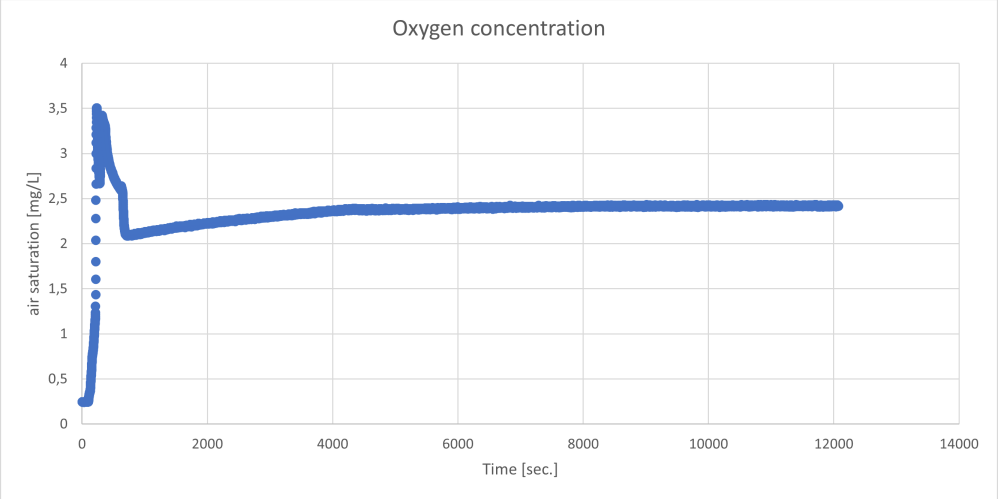

Figure B.3. Optic oxygen sensor measurement in 4/5 oxygen free demineralised water and 1/5 nanobubble water. The experiment was run on 13.12.2022

B.3 Optic oxygen sensor measurement in demineralised water on 08.02.2023

Calibration data 08.02.23

Table B.3. Calibration data to the optic oxygen sensor, 08.02.2023. N is the N moving average. LO = low and HI = high. sat = saturation.

N	**LO phase** [r.U.]	**HI phase** [r.U.]	**LO oxygen** [% air sat.]	**HI oxygen** [% air sat.]	**LO temp.** [$°C$]	**HI temp.** [$°C$]
3	58.74	27.83	0	100	19.76	20

The optic oxygen sensor measurement is made with the same parameters as the experiment made on 13.12.2022, but the experiment run is approximately 45 minutes compared to the three hours on the 13.12.2022. This time the experiments run time is shortened as it is seen from the data from the 13.12.2022 that the oxygen content does not change after approximately 45 minutes.

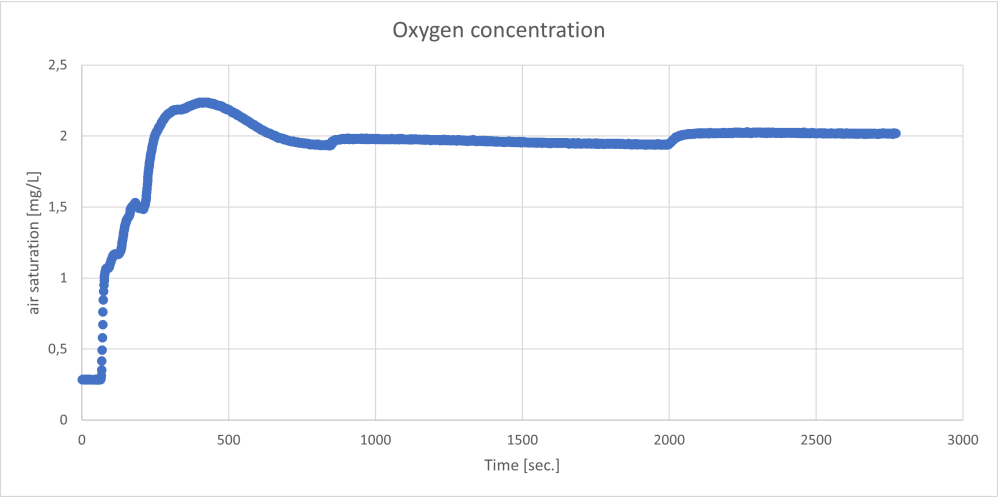

Figure B.4. Optic oxygen sensor measurement in 4/5 oxygen free demineralised water and 1/5 nanobubble water. The experiment was run on 08.02.2023

C Basic measurement

Every time the nanobubble generator was used there were taken samples out for different analysis, e.g. size distribution, zeta potential measurements and basic measurements. The basic measurements was made in order to see if they changed over time and are dissolved oxygen, temperature, redox potential, conductivity and pH.

Equipment:

- **WTW multi 3430** was used for dissolved oxygen, temperature, conductivity and pH [Xylem, 2015].
- **Mettler toledo elma 795** was used for redox potential [Elma Instruments, n/a].

Procedure:

1. Fill barrel up with water and connect gas type to the nanobubble generator.
2. Turn on the nanobubble generator on.
3. Take samples every 15 minutes (or other time interval).
4. Note down the basic measurement at each time step
5. Continue until needed.

Each table in this Appendix shows the dissolved oxygen measured, the saturated oxygen concentration (calculated from the measured temperature), the temperature, the redox potential, the conductivity and the pH-value at different time steps and different days.

The basic measurements are made over many various days and with different parameters, in order to find the most consistent conditions for producing the smallest nanobubbles. The measurements are divided into four categories:

1. Demineralised water and atmospheric air
2. BOD water and atmospheric air
3. Demineralised water and oxygen
4. BOD water and oxygen

BOD water is made with a mixture of different salts, and is called BOD water as it is normally used to BOD test for water. The BOD water contains calcium chloride dihydrate, ferric chloride hexahydrate, magnesium sulfate heptahydrate and a phosphate buffer [Cole-Parmer, n/a]. For calculations of amount added in order to make the solutions see Excel sheet '2. BOD solutions'.

The BOD water is used to ensure the most optimal conditions and making the experiments as close to wastewater as possible [Moleaer, n/a]. This can be seen in the data with the demineralised water as the basic measurements tend to fluctuate more and not a consistence tendency.

C.1 Demineralised water and atmospheric air

As the results in Table C.1 to C.3 shows, there is very little consistency with the basic measurements. An explanation for this could be, because all of the samples are taken in demineralised water, and it can be difficult to get accurate measurement of the parameters measured. Especially pH-values and redox potential are hard to measure in demineralised water. This was shown as it was very hard for the sensors to stabilise the values at any given time step. In table C.3 at time 120 mins, the measured dissolved oxygen exceed the saturated oxygen content as the only measurement of dissolved oxygen with the combination of demineralised water and atmospheric air.

Table C.1. The basic measurement taken on 14.12.2022 in demineralised water and atmospheric air. RP = Redox potential. sat = saturated. Waterflow = 75.7 L/min. Waterpressure = 1.2 bar. Gasflow = 0.05 L/min. Gaspressure = 0.9 bar.

Time [min.]	O_2 [mg/L]	O_2 **sat.** [mg/L]	**Temperature** [$°C$]	**RP** [mv]	**Conductivity** [$\mu S/cm$]	**pH** [-]
0	7.9	8.7	22.1	350	0.7	6.1
10	8.1	8.8	21.7	400	0.6	6.5
20	8.2	8.8	21.9	410	0.6	6.1
30	8.4	8.9	21.1	414	0.6	5.9
45	8.6	8.7	22.3	345	0.7	6.1
60	8.6	8.7	22.5	357	0.7	6.1

Table C.2. The basic measurement taken on 20.12.2022 in demineralised water and with atmospheric air. RP = Redox potential. sat = saturated. Waterflow = 75.7 L/min. Waterpressure = 1.2 bar. Gasflow = 0.05 L/min. Gaspressure = 0.9 bar.

Time [min.]	O_2 [mg/L]	O_2 **sat.** [mg/L]	**Temperature** [$°C$]	**RP** [mv]	**Conductivity** [$\mu S/cm$]	**pH** [-]
0	7.8	9.4	18.5	390	1	5.4
15	8.6	9.4	18.4	432	0.8	5.6
30	8.9	9.3	18.8	398	0.8	5.9
45	9.1	9.3	19.1	380	0.8	6.0
60	9.2	9.2	19.4	370	0.8	5.9

Table C.3. The basic measurement taken on 21.12.2022 in demineralised water and atmospheric air. RP = Redox potential. sat = saturated. Waterflow = 75.7 L/min. Waterpressure = 1.2 bar. Gasflow = 0.05 L/min. Gaspressure = 0.9 bar

Time [min.]	O_2 [mg/L]	O_2 **sat.** [mg/L]	**Temperature** [$°C$]	**RP** [mv]	**Conductivity** [$\mu S/cm$]	**pH** [-]
0	7.9	9.5	17.8	427	0.8	7.7
15	8.6	9.5	17.8	471	0.7	5.5
30	8.9	9.5	18.1	402	0.8	7.0
45	9.1	9.4	18.5	453	0.8	5.7
60	9.3	9.3	18.8	395	0.8	5.5
120	9.3	9.1	20.1	420	0.9	5.3

C.2 BOD water and atmospheric air

There is a clearer tendency in the basic measurements with the BOD solution in the demineralised water, compared to demineralised water, as seen in Table C.4 to C.7. The pH-value is stable at approximately 7 because of the pH-buffer. The reason for the slight different in pH variation from date to date in the experiments can be explained by the fact that the barrel is roughly 220 L i.e. the exact volume is not known. With atmospheric air and BOD water the oxygen content is just above saturation levels at approximately 60 min of run time for the nanobubble generator.

Table C.4. The basic measurement taken on 04.01.2023 in BOD water and atmospheric air. RP = Redox potential. sat = saturated. Waterflow = 75.7 L/min. Waterpressure = 1.2 bar. Gasflow = 0.05 L/min. Gaspressure = 0.9 bar

Time [min.]	O_2 [mg/L]	O_2 **sat.** [mg/L]	**Temperature** [$°C$]	**RP** [mv]	**Conductivity** [$\mu S/cm$]	**pH** [-]
0	7.8	9.3	19.0	247	80.2	7.2
15	8.4	9.2	19.3	260	80.7	7.5
30	8.7	9.2	19.5	254	80.7	7.5
45	8.9	9.1	19.9	255	80.5	7.5
60	9.0	9.1	20.2	257	80.4	7.5
90	9.0	9.0	20.8	255	80.7	7.4
120	9.0	8.9	21.4	265	80.2	7.4

Table C.5.The basic measurement 05.01.2023 in BOD water and with atmospheric air. RP = Redox potential. sat = saturated. Waterflow = 75.7 L/min. Waterpressure = 1.2 bar. Gasflow = 0.05 L/min. Gaspressure = 0.9 bar

Time [min.]	O_2 [mg/L]	O_2 **sat.** [mg/L]	**Temperature** [$°C$]	**RP** [mv]	**Conductivity** [$\mu S/cm$]	**pH** [-]
0	7.5	9.4	18.5	233	85.6	7.8
15	8.3	9.4	18.5	252	86.1	8.0
30	8.7	9.3	18.8	250	85.8	7.8
45	9.0	9.2	19.2	255	85.1	8.0
60	9.1	9.2	19.5	260	83.8	7.9
75	9.3	9.1	19.8	262	83.1	7.9
90	9.3	9.1	20.1	256	83.0	7.9
120	9.2	9.0	20.8	260	82.3	7.9

Table C.6.The basic measurement taken on 09.01.2023 in BOD water and atmospheric air. RP = Redox potential. sat = saturated. Waterflow = 75.7 L/min. Waterpressure = 1.2 bar. Gasflow = 0.05 L/min. Gaspressure = 0.9 bar

Time [min.]	O_2 [mg/L]	O_2 **sat.** [mg/L]	**Temperature** [$°C$]	**RP** [mv]	**Conductivity** [$\mu S/cm$]	**pH** [-]
0	7.5	9.0	20.7	234	79.9	7.0
15	8.1	9.0	20.5	247	83.5	7.4
30	8.4	9.0	20.8	247	83.3	7.4
45	8.6	8.9	21.1	250	83.2	7.4
60	8.7	8.9	21.3	250	83.5	7.4
75	8.8	8.8	21.6	255	83.1	7.4
90	8.9	8.8	21.9	253	83.4	7.4
120	8.8	8.7	22.4	253	83.1	7.4

Table C.7.The basic measurements taken on 10.01.2023 in BOD water and with atmospheric air. RP = Redox potential. sat = saturated. The redox potential sensor was broken. Waterflow = 75.7 L/min. Waterpressure = 1.2 bar. Gasflow = 0.05 L/min. Gaspressure = 0.9 bar

Time [min.]	O_2 [mg/L]	O_2 **sat.** [mg/L]	**Temperature** [$°C$]	**RP** [mv]	**Conductivity** [$\mu S/cm$]	**pH** [-]
0	7.6	9.4	18.6	-	83.1	7.3
15	8.4	9.4	18.6	-	85.3	7.4
30	8.8	9.3	18.9	-	85.3	7.4
45	9.0	9.2	19.4	-	85.3	7.4
60	9.2	9.2	19.6	-	85.2	7.4
75	9.2	9.1	20.0	-	85.3	7.4
105	9.2	8.9	20.9	-	85.0	7.3

C.3 Demineralised water and oxygen

As Table C.8 shows are the only major difference in demineralised water and oxygen compared to demineralised water and atmospheric air the dissolved oxygen. The dissolved oxygen content is well above saturation somewhere between 15 mins and 30 mins and is above the max range for the sensor used i.e. 20 mg/L.

Table C.8. The basic measurements taken on 21.02.2023 in demineralised water and with oxygen. RP = Redox potential. sat = saturated. OFL = outside measuring range, max = 20 mg/L. Waterflow = 75.7 L/min. Waterpressure = 1.2 bar. Gasflow = 0.05 L/min. Gaspressure = 0.9 bar

Time [min.]	O_2 [mg/L]	O_2 **sat.** [mg/L]	**Temperature** [$°C$]	**RP** [mv]	**Conductivity** [$\mu S/cm$]	**pH** [-]
0	7.5	9.2	19.7	291	0.5	6.5
15	15.3	9.2	19.6	305	1.3	5.4
30	OFL	9.1	20.0	354	1.3	5.5
45	OFL	9.0	20.3	373	1.3	5.5
60	OFL	9.0	20.6	355	1.3	5.5
75	OFL	8.9	21.0	378	1.3	5.4
90	OFL	8.9	21.3	377	1.3	5.7

C.4 BOD water and oxygen

Table C.9 to C.13 shows the basic measurements for BOD water and oxygen. Here the dissolved oxygen content is well above the saturated level and is acheived between 15 and 30 mins as for demineralised water and oxygen.

Table C.9. The basic measurements taken on 27.02.2023 in BOD water and with oxygen. RP = Redox potential. sat = saturated. OFL = outside measuring range, max = 20 mg/L. Waterflow = 75.7 L/min. Waterpressure = 1.2 bar. Gasflow = 0.05 L/min. Gaspressure = 0.9 bar

Time [min.]	O_2 [mg/L]	O_2 **sat.** [mg/L]	**Temperature** [$°C$]	**RP** [mv]	**Conductivity** [$\mu S/cm$]	**pH** [-]
0	7.9	9.5	17.8	306	84.9	7.3
15	16.3	9.5	17.8	337	82.9	7.3
30	OFL	9.4	18.2	346	83.1	7.4
45	OFL	9.4	18.6	350	83.2	7.4
60	OFL	9.3	18.9	355	83.1	7.4
75	OFL	9.2	19.3	357	82.7	7.4
90	OFL	9.2	19.6	362	82.5	7.3

Table C.10. The basic measurements taken on 28.02.2023 in BOD water and with oxygen. RP = Redox potential. sat = saturated. OFL = outside measuring range, max = 20 mg/L. Waterflow = 75.7 L/min. Waterpressure = 1.2 bar. Gasflow = 0.05 L/min. Gaspressure = 0.9 bar

Time [min.]	O_2 [mg/L]	O_2 **sat.** [mg/L]	**Temperature** [$°C$]	**RP** [mv]	**Conductivity** [$\mu S/cm$]	**pH** [-]
0	7.8	9.2	19.4	273	84.5	7.2
15	16.7	9.2	19.3	314	86.7	7.5
30	OFL	9.2	19.5	332	86.1	7.4
45	OFL	9.1	19.8	344	85.3	7.4
60	OFL	9.1	20.1	345	84.4	7.4
75	OFL	9.0	20.4	349	83.2	7.4
90	OFL	9.0	20.7	352	82.5	7.4

Table C.11. The basic measurements taken on 14.03.2023 in BOD water and with oxygen. RP = Redox potential. sat = saturated. OFL = outside measuring range, max = 20 mg/L. pH sensor was defect on this day of measurement, therefore no pH-values taken. Waterflow = 75.7 L/min. Waterpressure = 1.2 bar. Gasflow = 0.1 L/min. Gaspressure = 0.95 bar

Time [min.]	O_2 [mg/L]	O_2 **sat.** [mg/L]	**Temperature** [$°C$]	**RP** [mv]	**Conductivity** [$\mu S/cm$]	**pH** [-]
0	7.6	9.6	17.4	277	83.7	-
15	16.4	9.5	17.7	318	82.6	-
30	OFL	9.5	18.1	339	81.0	-
45	OFL	9.4	18.4	347	79.5	-
60	OFL	9.3	18.8	352	78.2	-
75	OFL	9.3	19.1	360	77.4	-
90	OFL	9.2	19.5	362	77.0	-

Table C.12. The basic measurements taken on 21.03.2023 in BOD water and with oxygen. RP = Redox potential. sat = saturated. OFL = outside measuring range, max = 20 mg/L. Waterflow = 75.7 L/min. Waterpressure = 1.2 bar. Gasflow = 0.05 L/min. Gaspressure = 0.9 bar

Time [min.]	O_2 [mg/L]	O_2 **sat.** [mg/L]	**Temperature** [$°C$]	**RP** [mv]	**Conductivity** [$\mu S/cm$]	**pH** [-]
0	7.5	9.3	19.0	254	81.9	7.1
15	14.9	9.3	18.9	308	81.7	7.3
30	OFL	9.2	19.2	330	81.6	7.3
45	OFL	9.2	19.5	344	80.9	7.3
60	OFL	9.1	19.9	351	79.5	7.3
75	OFL	9.1	20.2	349	78.9	7.3
90	OFL	9.0	20.5	357	77.9	7.4

Table C.13. The basic measurements taken on 22.03.2023 in BOD water and with oxygen. RP = Redox potential. sat = saturated. OFL = outside measuring range, max = 20 mg/L. Waterflow = 75.7 L/min. Waterpressure = 1.2 bar. Gasflow = 0.05 L/min. Gaspressure = 0.9 bar

Time [min.]	O_2 [mg/L]	O_2 **sat.** [mg/L]	**Temperature** [$°C$]	**RP** [mv]	**Conductivity** [$\mu S/cm$]	**pH** [-]
0	7.7	9.4	18.3	270	81.6	7.2
15	15.3	9.4	18.4	311	83.7	7.3
30	18.7	9.3	18.7	327	82.9	7.3
45	OFL	9.3	19.0	339	81.8	7.3
60	OFL	9.2	19.3	344	80.9	7.3
75	OFL	9.2	19.7	347	79.2	7.3
90	OFL	9.1	20.1	348	79.8	7.3

D Documentation of hydroxyl radicals - Fenton Reaction, methylene blue dye and benzoic acid

D.1 The Fenton reaction

Equipment:
Mettler Toledo Seven Multi pH meter
SI Electronics pH electrode
Sartorius BP221S scale
Pipette 1-5 mL
Magnetic stirrer
Measuring cylinders
beakers

Software:
Cary WinUV Software (Scan)

Chemicals:
Iron(II) sulfate heptahydrate, $FeSO_4{:}7H_2O$ (CAS: 7782-63-0)
33% Hydrogen peroxide (unstabilised), H_2O_2 (CAS:7722-84-1)
12 M Hydrochloric acid, HCl (CAS: 7647-01-0)

Procedure:

1. 12 M hydrochloric acid is dilued to 1 M in a beaker
2. Another beaker containing 100 mL demineralised water is placed on a magnetic stirrer and 0.22 g iron(II)sulfate heptahydrate is added during stirring.
3. The pH of the solution is lowered to 3 by adding 1 M hydrochloric acid and observing the pH on a meter.
4. The hydrogen peroxide is diluted to 3% in a separate beaker
5. The Fenton reaction will begin when the 3% hydrogen peroxide is added to the beaker containing iron(II)sulfate heptahydrate (pH 3)

For the experiment unstabilised hydrogen peroxide was used as some of the stabilisers can act as hydroxyl radical scavengers [Satoh et al., 2007]. Furthermore it was diluted to 3% as high concentrations may affect results [Satoh et al., 2007].

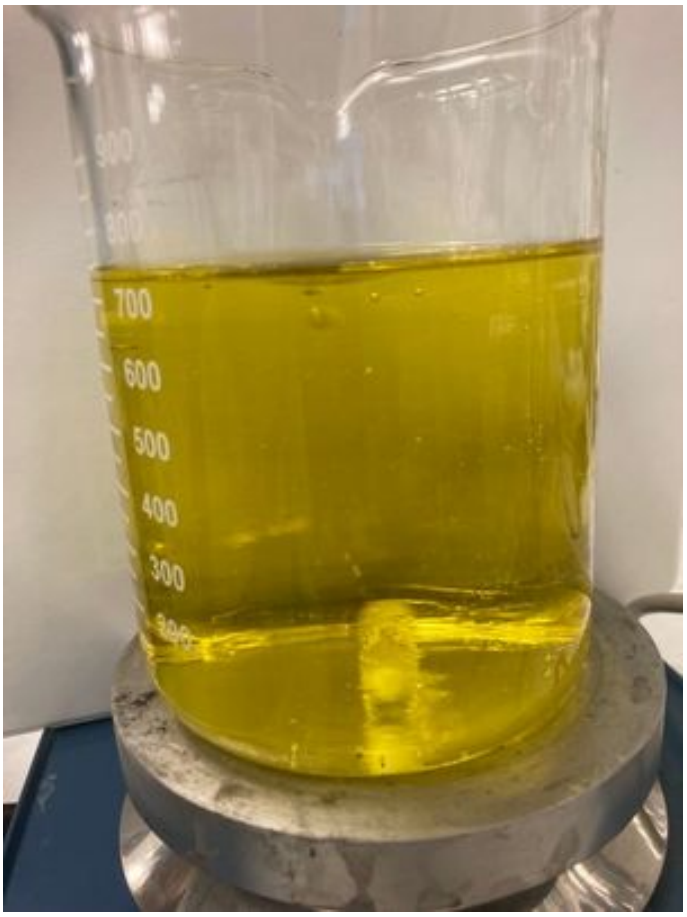

Figure D.1.Fenton reaction after adding hydrogen peroxide 3% to the iron(II) sulfate heptahydrate solution.

The Fenton reaction forms hydroxyl radicals and is used for testing if hydroxyl radicals can degrade methylene blue.

D.2 Methylene blue

Two methylene blue experiments were conducted in this project: (1) testing if hydroxyl radicals in the Fenton reaction can degrade methylene blue and (2) testing if methylene blue can be degraded by circulation, nanobubbles, UV light or a combination of UV light and nanobubbles.

D.2.1 Degradation of methylene blue - Fenton reaction

Equipment:
Varian Cary 50 UV-VIS photometer
Polystyrene cuvettes 10x10x45 mm
Sartorius BP221S scale
Pipette 1-5 mL
Pipette 100-1000 μL
Magnetic stirrer

Software:
Cary WinUV Software (Scan)

Chemicals:
Methylene blue, $C_{16}H_{18}N_3SCl$ (CAS: 61-73-4)

To separate the degradation effects on methylene blue, of each component in the Fenton reaction, four experiments were conducted:

1. Iron(II)sulfate adjusted to pH 3
2. Hydrogen peroxide 3%
3. Methylene blue only
4. The Fenton reaction

Iron(II)sulfate heptahydrate, hydrogen peroxide and the Fenton reation are all prepared as described in D.1.

Procedure:

- All of the experiments were circulated on a magnetic stirrer
- For each of the experiments methylene blue was added to reach a final methylene blue concentration of 0.16 mM. For experiment (3) 0.01 g methylene blue is dissolved in 200 mL demineralised water.
- For experiment (4) methylene blue was added following the pH adjustment of iron(II)sulfate.
- For each experiment the solution is sampled at 0 and 5 minutes
- Initially 250 μL sample was diluted in a cuvette with 1.25 mL demineralised water. Ideally 148 μL is diluted in 1.5 mL to reach an absorbance baseline of 1.
- Absorbance is measured in the range from 500 to 700 nm. Peak absorbance of methylene blue is at 665 nm.

No reduction in the methylene blue absorbance was registered in the samples containing iron(II)sulfate, hydrogen peroxide or methylene blue only. However, for the Fenton reaction - combining iron(II)sulfate and hydrogen peroxide to form hydroxyl radicals - the methylene blue was completely degraded after 5 minutes, see Figure D.2. The 0 minute sample for the Fenton reaction (experiment 4) was sampled immediately after adding the hydrogen peroxide to the solution of iron(II)sulfate and methylene blue, but still the reduction is visible on the graph.

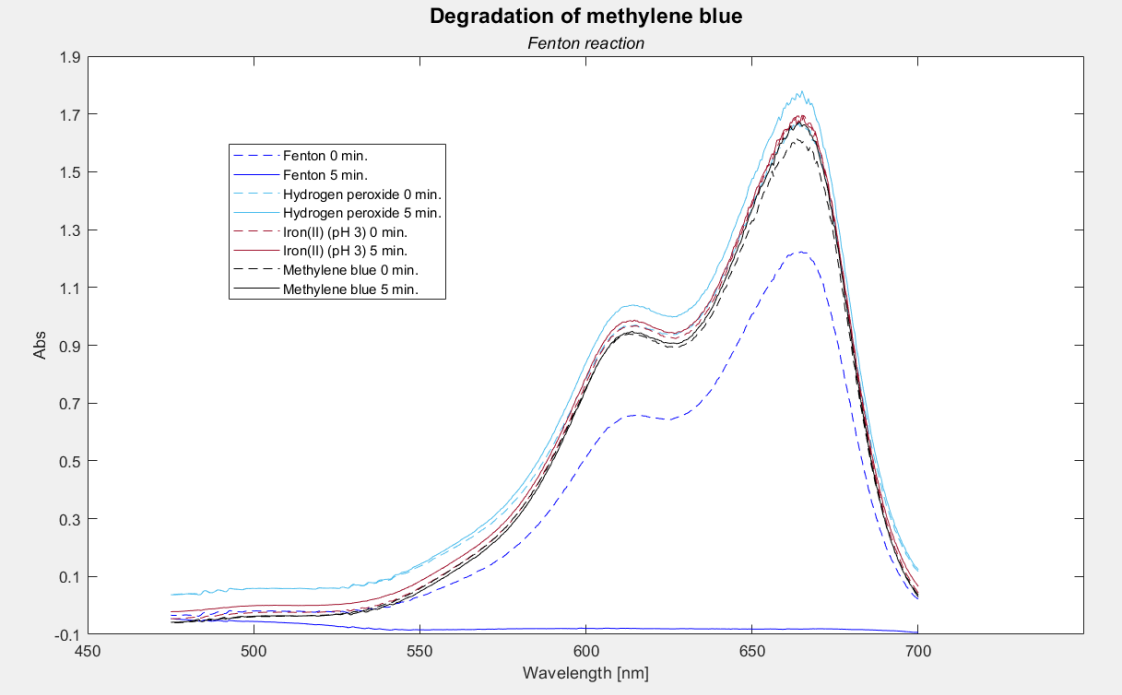

Figure D.2.Degradation of methylene blue using; (1) Iron(II)sulfate (2) Hydrogen peroxide 3% (3) the Fenton reaction as well as a sample of (4) methylene blue only. The methylene blue peak is at 665 nm. Only for the Fenton at five minutes has all methylene blue been degraded.

All results can be found in Excel sheet 'A1. Methylene blue experiments (Fenton reaction)'.

D.2.2 Degradation of methylene blue - nanobubbles and UV

The experimental setup for these experiments have already been described in Section 3.3. This is an elaboration of the procedure for the experiments.

Equipment:
Varian Cary 50 UV-VIS photometer
Polystyrene cuvettes 10x10x45 mm
Ecoline VC-380 peristaltic pump
Multi UV-C 254nm 3W chamber/lamp
Sartorius BP221S scale
Pipette 1-5 mL
Pipette 100-1000 μL
Magnetic stirrer Volumetric flasks
250 mL Bluecap bottle
Lid for bluecap bottle fitted to tubes connected to UV chamber and pump
50 mm tube
100 mm tube

Software:
Cary WinUV Software (Scan)

Chemicals:
Methylene blue, $C_{16}H_{18}N_3SCl$ (CAS: 61-73-4)
BOD solutions, see Excel sheet '2 BOD solutions'

Procedure:

1. A 250 mL bluecap bottle containing a magnet is placed on a magnetic stirrer
2. BOD water or nanobubble water is poured into a 50 mL and 100 mL volumetric flask (dependping on experiment)
3. The 50 mL volumetric flask is emptied into the bluecap bottle and the magnetic stirrer is started at 150 rpm
4. 0.0075 g methylene blue is added to the bluecap bottle and the weighing tray is rinsed with water from the 100 mL volumetric flask using a pipette before the rest of the 100 mL volumetric flask is emptied into the bluecap bottle
5. The stirring is increased to 300 rmp
6. To ensure complete mixing the content of the bluecap bottle is stirred for 2 minutes before a sample is collected (at 0 min.)
7. The bluecapbottle is closed with cap and tubes
8. The UV lamp is connected and turned on
9. The pump is started at frequency 30 and the timer is set to 10 min
10. A 1.5 mL sample is collected from the bluecap bottle every 15 minutes
11. 148 μL is pipetted into eight cuvettes and diluted with 1.5 mL BOD solution.
12. The eight cuvettes are scanned at 665 nm

D.2.3 Absorbance spectra and standard curve

Standard absorbance curve for methylene blue

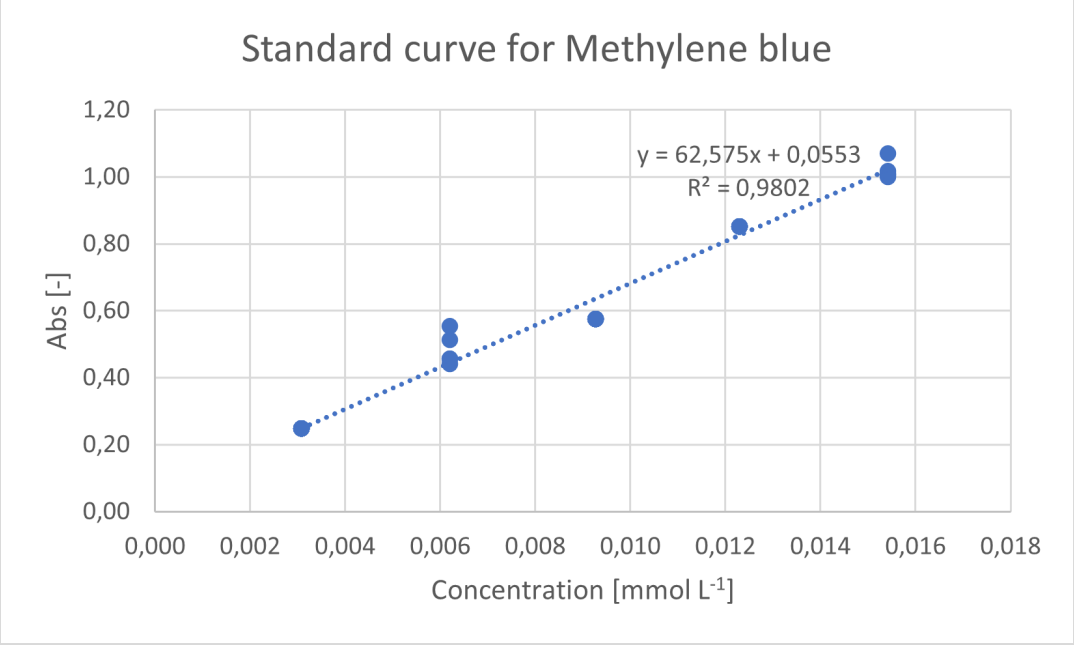

Figure D.3.Standard curve for methylene blue experiments with a concentration of 0.0157 mM.

Methylene blue has three absorption spectra of of which only the one at 665 nm was measured, see figure D.4.

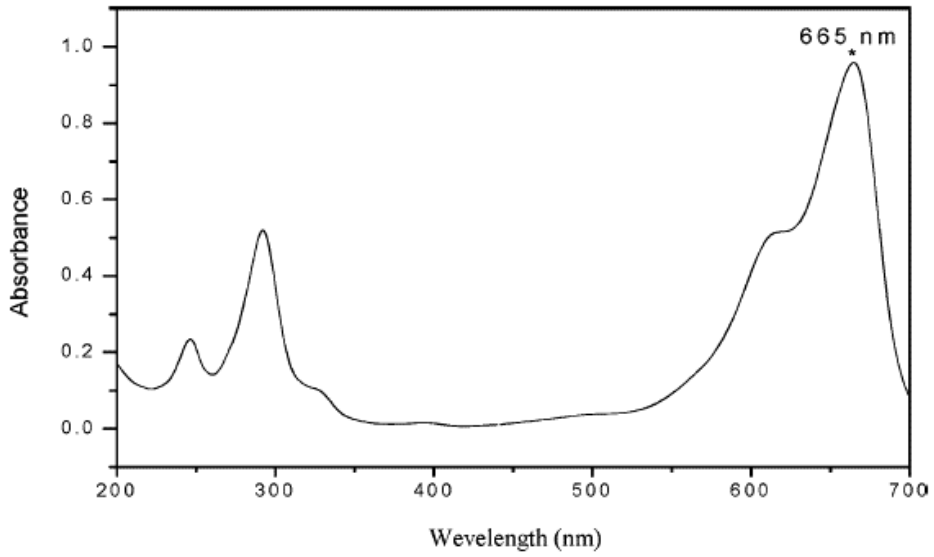

Figure D.4.Absorption spectra of Methylene blue be treatment. Concentration 50 mg/L [Melgoza et al., 2009].

D.3 Benzoic acid

Equipment:
Varian Cary 50 UV-VIS photometer
Polystyrene cuvettes 10x10x45 mm
Sartorius BP221S scale
Pipette 1-5 mL
Pipette 100-1000 μL
Magnetic stirrer Beakers

Software:
Cary WinUV Software (Scan)

Chemicals:
Benzoic acid, $C_7H_6O_2$ (CAS: 65-85-0)

Procedure:

1. The Fenton reaction is initiated while the magnetic stirrer is switched on, as described in Section D.1
2. Immediately after initiating the Fenton reaction benzoic acid is added to corresponding to a molarity of 9 mM
3. Most of the benzoic acid will remain undissolved on top of Fention reaction and is only gradually dissolved
4. 2 mL of the solution is pipetted into a cuvette

As the Fenton reaction degrades the benzoic acid, an iron complex should form resulting in an absorbance peak at 517 nm and a visible discolouration, but this was not observed, see Figure D.5. Iron(II) and a pH at 3 is a prerequisite for the iron complex to form [Satoh et al., 2007].

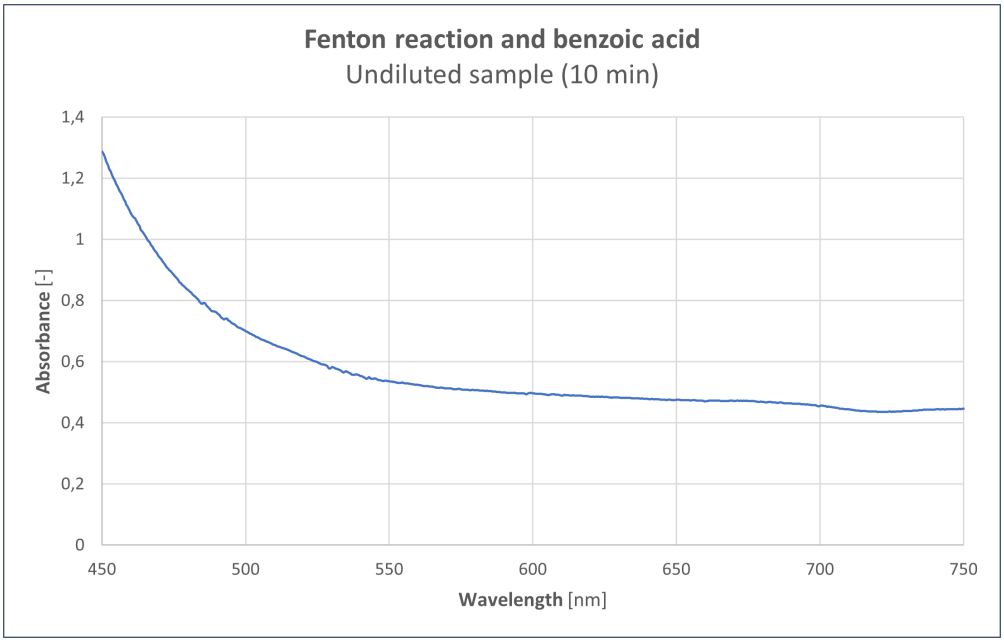

Figure D.5. Benzoic acid absorbance sampled 10 minutes after the initiation of the Fenton reaction. Absorbance for 2 mL undiluted sample - 03.01.2023

Benzoic acid has two absorbance peaks between 200 and 300 nm, but due to the low solubility of benzoic acid in water, there will be no baseline for the absorbance.

All results can be found in Excel sheet 'A2. Benzoic acid experiments (Fenton reaction)'.

E Standard curves for Diclofenac and Venlafaxine

Figure E.1 shows the standard curve made for diclofenac as well as a theoretical standard curve. The theoretical standard curve are based on the area found with the HPLC at a concentration of 100 mg/L (or the same as 100%) and then calculated downwards to 10 % i.e. 10 mg/L. The figure shows that there is a perfect correlation between the measured and the theoretical standard curve.

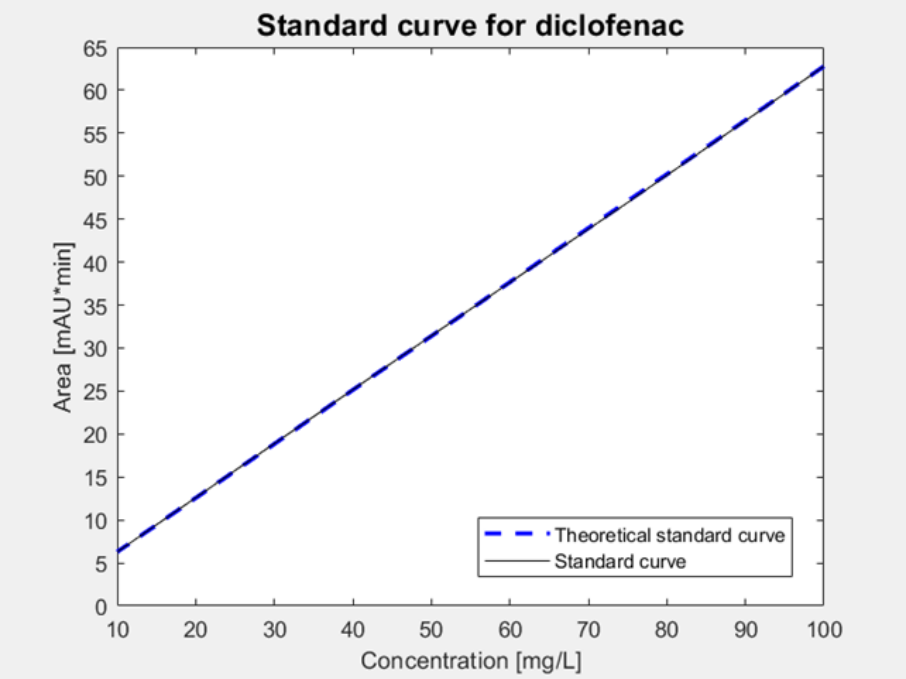

Figure E.1.Standard curve for diclofenac.

Figure E.2 shows the standard curve made for venlafaxine as well as a theoretical standard curve. The theoretical standard curve are based on the area found with the HPLC at a concentration of 100 mg/L (or the same as 100%) and then calculated downwards to 10 % i.e. 10 mg/L. Even though there are a slight deviation of the measured area compared to the theoretical at the different concentrations it is concluded that the standard curve is still within acceptable range.

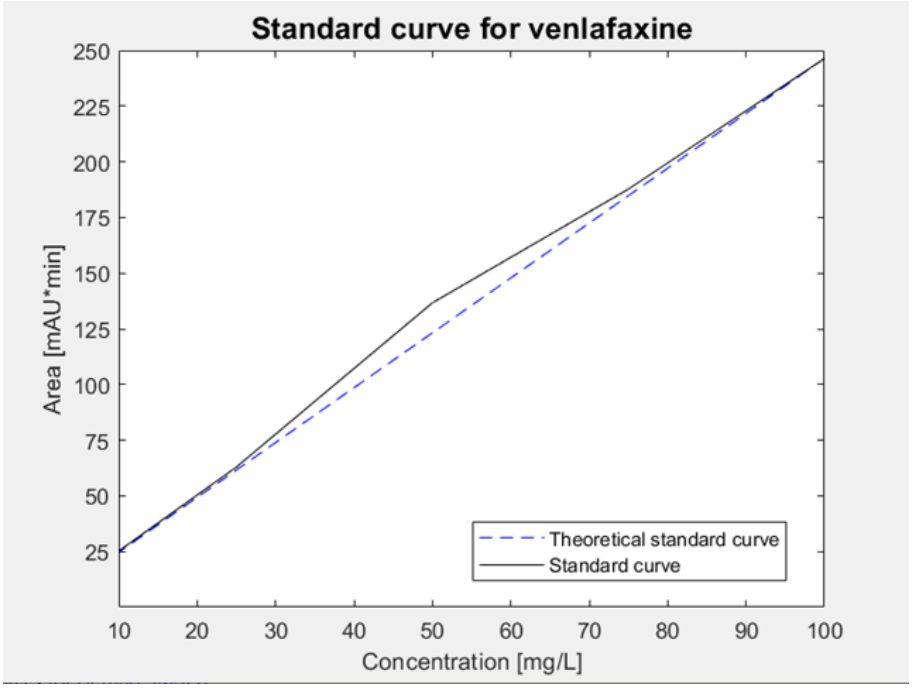

Figure E.2.Standard curve for venlafaxine.

F Redox potential

Figure F.1 to F.4 shows the redox potential as a function of time made in the four different categories, i.e. demineralised water and atmospheric air, BOD water and atmospheric air, demineralised water and oxygen and BOD water and oxygen.

Figure F.1 shows no consistency in redox potential as a function of time in demineralised water and atmospheric air. This only supports the notion stated in the project that experiments in demineralised water does not yield the best results.

Figure F.2 shows the redox potential over time with BOD water and atmospheric air. This shows a more clear increasing tendency than in demineralised water and atmospheric air but the measurement still fluctuates from timestep to timestep.

Figure F.3 shows an increasing trend in the redox potential over time for demineralised water in combination with oxygen. This shows again that there is a more clear increasing tendency in the redox potential but it still varies from time step to time step.

Figure F.4 shows that in BOD water and oxygen there is a consistent increasing trend in redox potential over time.

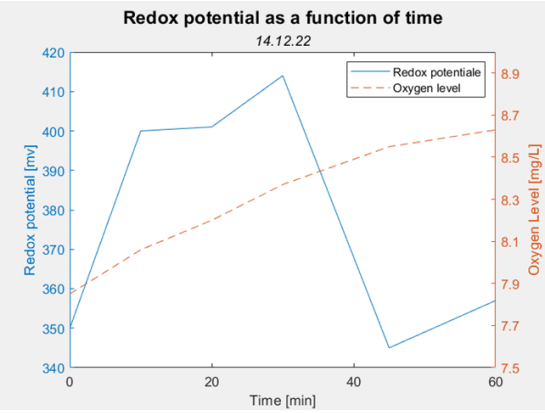

Figure F.1.14.12.22 - Redox potential as a function of time. Demineralised water and atmospheric air.

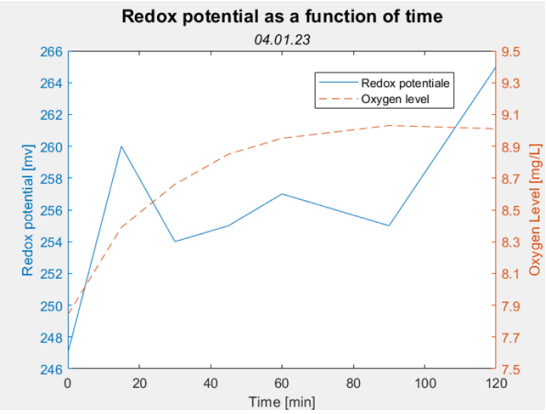

Figure F.2.04.01.23 - Redox potential as a function of time. BOD water and atmospheric air.

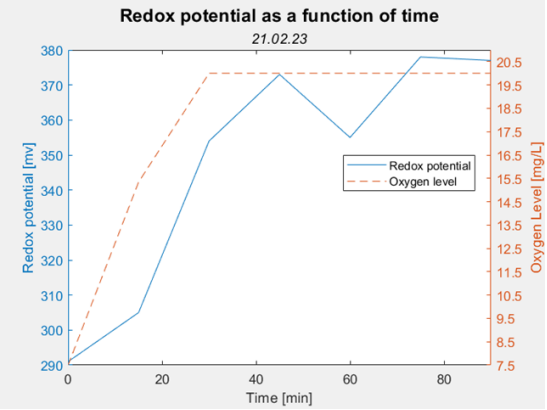

Figure F.3.21.02.23 - Redox potential as a function of time. Demineralised water and oxygen.

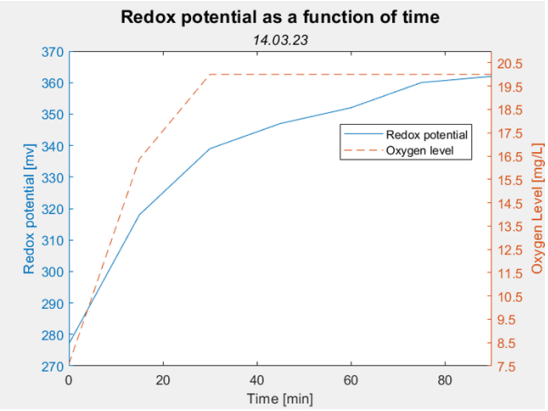

Figure F.4.14.03.23 - Redox potential as a function of time. BOD water and oxygen.

G Chemical structures

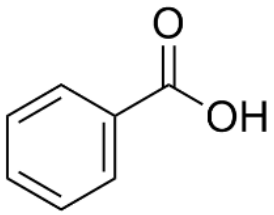

Figure G.1.Chemical structure of benzoic acid [ChemSrc, n/a].

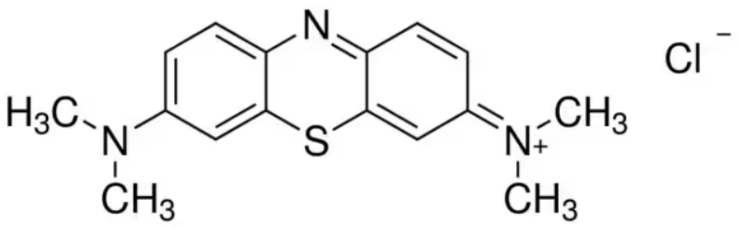

Figure G.2.Chemical structure of methylene blue [Merck, n/ab].

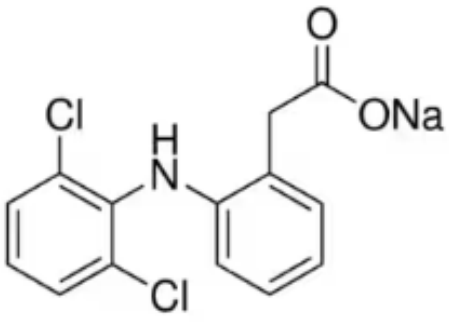

Figure G.3.Chemical structure of diclofenac sodium salt [Merck, n/aa].

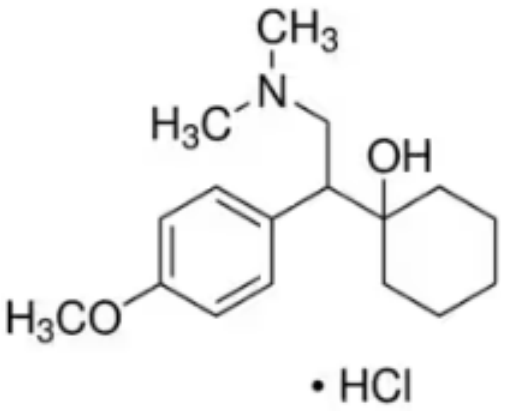

Figure G.4.Chemical structure of venlafaxine hydrochloride [Merck, n/ac].